213325-3-F

Final Report

HOLOGRAPHIC LENS FOR WIDE FIELD-OF-VIEW LASER COMMUNICATION RECEIVER

A. TAI
M. EISMANN
B. NEAGLE

Environmental Research Institute of Michigan
Optical Science Laboratory
Advanced Concepts Division

MARCH 1990

Sponsored by:
USAF Wright Research and Development Center
WRDC/AAAI-2
Wright Patterson AFB, OH 45433

UNCLASSIFIED

SECURITY CLASSIFICATION OF THIS PAGE

REPORT DOCUMENTATION PAGE

Form Approved OMB No. 0704-0188

1a REPORT SECURITY CLASSIFICATION: Unclassified

1b RESTRICTIVE MARKINGS:

2a SECURITY CLASSIFICATION AUTHORITY:

2b DECLASSIFICATION/DOWNGRADING SCHEDULE:

3 DISTRIBUTION/AVAILABILITY OF REPORT:

4 PERFORMING ORGANIZATION REPORT NUMBER(S): 213325-3-F

5 MONITORING ORGANIZATION REPORT NUMBER(S):

6a NAME OF PERFORMING ORGANIZATION: Environmental Research Institute of Michigan

6b OFFICE SYMBOL (if applicable):

7a NAME OF MONITORING ORGANIZATION: Infrared Information Analysis Center

6c ADDRESS (City, State, and ZIP Code): P.O. Box 8618, Ann Arbor, MI 48107

7b ADDRESS (City, State, and ZIP Code): P.O. Box 8618, Ann Arbor, MI 48107

8a NAME OF FUNDING/SPONSORING ORGANIZATION: AF WRDC/AAAI-2

8b OFFICE SYMBOL (if applicable):

9 PROCUREMENT INSTRUMENT IDENTIFICATION NUMBER: DLA900-88-D-0392/004

8c ADDRESS (City, State, and ZIP Code): USAF Wright Research & Development. WRDC/AAAI-2, Wright Patterson AFB, OH 45433

10 SOURCE OF FUNDING NUMBERS

PROGRAM ELEMENT NO	PROJECT NO	TASK NO	WORK UNIT ACCESSION NO

11 TITLE (Include Security Classification): Holographic Lens for Wide Field-of-View Laser Communication Receiver

12 PERSONAL AUTHOR(S): A. Tai, M. Eismann and B. Neagle

13a TYPE OF REPORT	13b TIME COVERED	14 DATE OF REPORT (Year, Month, Day)	15 PAGE COUNT
Final Technical	FROM 5/1/89 TO 12/31/89	March 1990	

16 SUPPLEMENTARY NOTATION:

17 COSATI CODES			18 SUBJECT TERMS (Continue on reverse if necessary and identify by block number)
FIELD	GROUP	SUB-GROUP	

19 ABSTRACT (Continue on reverse if necessary and identify by block number)

In this report, the design and fabrication of a wide field-of-view (FOV) holographic lens for use in a laser receiver are described. The holographic lens is designed to image incoming laser radiation at 850 nm onto a solid state detector array over a field-of-view of $\pm 22.5^{o} \times \pm 16^{o}$ ($\pm 26.7^{o}$ in the diagonal direction). Experimental results obtained with the holographic wide FOV laser receiver are presented. The location of the focussed spot can be determined to within one pixel of the detector array, providing the laser receiver with an angular resolution better than 1 mrad.

20 DISTRIBUTION/AVAILABILITY OF ABSTRACT: XX UNCLASSIFIED/UNLIMITED ☐ SAME AS RPT ☐ DTIC USERS

21 ABSTRACT SECURITY CLASSIFICATION: Unclassified

22a NAME OF RESPONSIBLE INDIVIDUAL: Mr. Gary Wilkins

22b TELEPHONE (Include Area Code):

22c OFFICE SYMBOL: WRDC/AAAI-2

DD Form 1473, JUN 86 *Previous editions are obsolete.*

ERIM 116

UNCLASSIFIED

SECURITY CLASSIFICATION OF THIS PAGE

PREFACE

This report is prepared by the Optical Science Laboratory, Advanced Concepts Division of the Environmental Research Institute of Michigan. The work was sponsored by USAF Wright Research and Development Center, WRDC/AAAI-2 (Communication Technology) through the Infrared Information Analysis Center under contract DLA900-88-D-0392/004.

This report covers work performed between May 1, 1989 and December 31, 1989. The principal investigator was Anthony Tai and the major contributors to this effort were Anthony Tai, Michael Eismann and Bradley Neagle.

This page intentionally left blank.

TABLE OF CONTENTS

This page intentionally left blank.

LIST OF FIGURES

LIST OF FIGURES (Continued)

1.0 INTRODUCTION

This report describes the design and fabrication of a holographic lens for use in a wide field-of-view (FOV) laser communication receiver. The work was funded by WRDC/AAAI-2 through IRIA under contract DLA900-88-D-0392/004.

In air-to-air laser communication between two aircraft, the transmitters and receivers on the aircraft must be able to track each other continuously. The tracking systems can be implemented with various position sensing devices but to maximize tracking precision, their FOVs must be fairly narrow. A separate acquisition system with a wide FOV is therefore needed to initially locate the other aircraft and it must provide enough accuracy to bring the laser transmitter/receiver to within the FOV of the tracking system.

In the acquisition mode, the transmitted laser beams from the two aircraft are both scanned over a wide pattern while the wide FOV receivers search for and determine the location of incoming laser radiation. When laser radiation is detected and its angular position is determined, the transmitter reduces the size of the scan pattern and centers the scan at the location of the detected laser source on the other aircraft. At the same time, the tracking receiver is steered towards the laser radiation emitted from the other aircraft until it is within the FOV of the tracker.

To detect and determine the angular position of incoming laser radiation, it was proposed that a wide angle lens be used to image a wide area scene onto a solid state detector array through a narrow band spectral filter. The location of the focussed spot at the setector array will provide the location of the laser source. There are several design issues that must be considered in selecting the implementation approach. First, the laser communication system is to be carried on an

aircraft and several may be needed around the platform to cover a full 4π steradian. A light weight and compact design is therefore crucial. Second, it is desirable for the laser receiver to have a minimal effect on the radar cross-section of the aircraft. Finally, it is advantageous to have a versatile design approach that can be modified and extended to cover a wider FOV or to conform to other physical constraints. Holographic optics offers an attractive means to satisfy all of these design goals.

In Section 2 of this report, the system requirements of the wide FOV laser receiver are defined. An introduction to holographic optics is then given in Section 3 where the features of the holographic optics are discussed and the various fabrication techniques are described. The design approach for the wide FOV laser receiver is presented in Section 4 and the fabrication procedure for the holographic lens is given in Section 5. The experimental results obtained with the laser receiver are documented in Section 6. A summary of the work is provided in Section 7 together with suggestions for follow-on efforts.

2.0 SYSTEM REQUIREMENTS AND SPECIFICATIONS

The laser receiver is designed to detect and locate 850nm laser radiation over a FOV of about $\pm 22.5^{\circ}$ by imaging onto a CID detector array. A CID detector array was chosen because of its resistance to blooming as compared with CCD detector arrays. The unit chosen was a CIDTEC CID2710 camera. The detector array has a dimension of 9mm(Horizontal) x 6.6mm(Vertical). Since the detector array is rectangular, the lens was designed to image over a FOV of $\pm 22.5^{\circ}$(H) x $\pm 16^{\circ}$(V). The FOV in the diagonal direction is $\pm 26.7^{\circ}$. The imaging lens must therefore be able to provide adequate performance over a full FOV of 53.4°.

With a holographic lens, the FOV is related to the detector array size D and the focal length f by $FOV=2\sin^{-1}[D/2f]$. Thus, to cover a FOV of $\pm 22.5^{\circ}$ in the horizontal direction with a detector of size D=9mm, the focal length of the lens must be about 12mm. The effective aperture of the lens is defined by the limiting aperture as illustrated in Figure 1. The design goal is to achieve an effective f/number close to f/2. The full aperture of the lens, however, is determined by both the effective aperture and the FOV. With an effective aperture of f/2 and a $\pm 26.7^{\circ}$ FOV, the f/number of the lens over its full aperture is a very fast f/0.7.

The CID2710 has 755(H) x 484(V) pixels and the pixel size is 12μm(H) x 13.7μm(V). The detector output is digitized by a 512x512 frame grabber, resulting in an effective pixel size of approximately 17μm(H) x 13.7μm(V). For position sensing, the position of the focussed spot can only be determined to within $\pm 1/2$ a pixel if the spot size is smaller than the detector pixel as illustrated in Figure 2(a). However, if the spot is circularly symmetric and covers an area between one to two pixels, the centroid of the focussed spot can be determined to within a fraction of a pixel by interpolating the detector output as

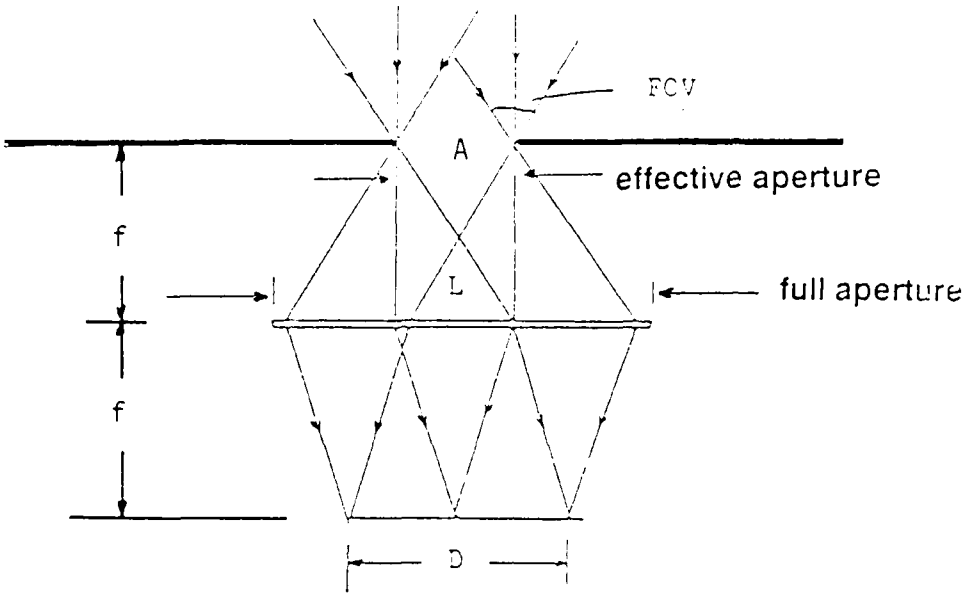

Figure 1. Geometry of Imaging System.

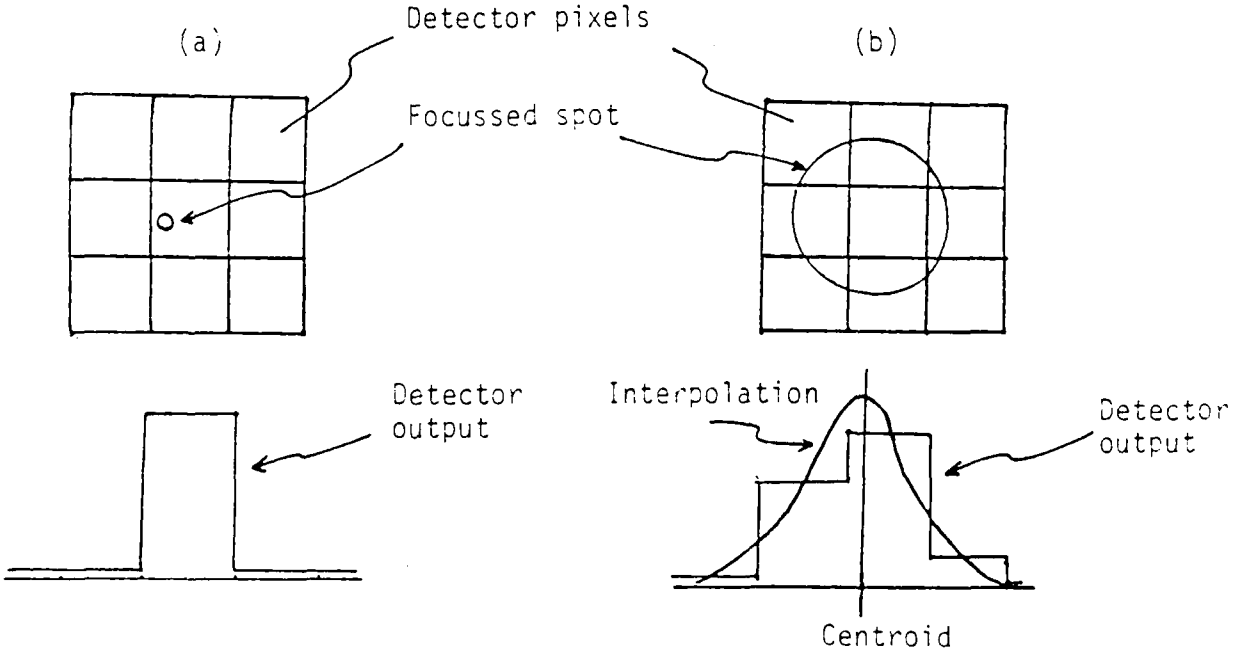

Figure 2. Determination of the location of the focussed spot.
(a) Spot size < pixel size, (b) Spot size between 1 to 2 pixels.

shown in Figure 2(b). Since the average pixel size of the detector after digitization is about 15μm, the design goal for the imaging lens is to produce a symmetric focussed spot of constant diameter somewhere between 15μm and 30μm in diameter for all incident beam angles within a $\pm 26.7^{\circ}$ FOV. With the spatial position of the laser source determined to within a fraction of a pixel, the angular resolution of the laser receiver is better than 1.1mrad (45°/512).

This page intentionally left blank.

3.0 HOLOGRAPHIC LENS

In this section, an introduction to holographic optical elements is presented. The purpose is to provide justification for the selection of a specific holographic design in the implementation of the laser receiver. The unique features offered by a holographic lens are first described and applications where holographic optics can provide distinct advantages over conventional optics are discussed. Various design and fabrication approaches for holographic lenses are then compared and the approach most suited for the implementation of the wide FOV holographic lens is selected.

3.1 Unique Features of Holographic Lenses

One of the most important applications of holographic optics is the fabrication of lenses for optical systems with special requirements that can not be easily met with conventional refractive and reflective optical elements. Holographic lenses offer several features that make them very attractive for these optical systems. 1) A conventional lens realizes the desired phase transformation by varying the thickness of an optical material to provide the total optical path difference. A holographic lens, on the other hand, provides the optical path difference modulo-2π and it does not rely solely on wavefront retardation by the thickness an optical material to produce the desired phase shift. A fast holographic lens with a large aperture can be fabricated on a flat substrate with just enough thickness to assure flatness. A holographic lens is therefore lighter and more compact than its refractive or reflective optical counterparts. The airborne wide FOV receiver for laser communication is one example where light weight and compactness are important design considerations. Diffractive optics used by itself or in conjunction with refractive lenses offers a means to significantly reduce the size and weight of such optical systems. 2) The phase function of a holographic lens is

defined by its spatial structure. It is easier to generate with high precision a 2-dimensional pattern than to control the 3-dimensional shape of a conventional lens. This is particularly true with lenses whose phase functions are decentered, asymmetric or aspherical as with the case of the wide angle lens. 3) More than one phase function can be multiplexed onto a diffractive lens by spatial frequency multiplexing or by spatial multiplexing. 4) By controlling the diffraction efficiency which can range from 0 to 100%, a holographic optical element can combine the functions of a beam splitter and a lens. A sample application is the implementation of taps in a laser communication system. 5) A reflection hologram is essentially a multilayer dielectric reflective spectral filter. A diffractive optical element can therefore combine the functions of a spectral filter and a lens into a single element. Using this feature, a laser receiver can, for example, be integrated with a conventional broadband (or white light) imager without having to compromise the efficiency of either system. 6) Holographic lenses with high spatial carrier frequencies disperse and focus light simultaneously, making them suitable for multiplexing and demultiplexing in wavelength-multiplexed optical communication systems. 7) A holographic lens exhibits chromatic aberration with a sign opposite that of a refractive lens, making it possible to fabricate a compact achromatic lens by etching a diffractive element onto a refractive lens.

One or more of these unique features provided by holographic optics can, in many optical systems, offer significant operational advantages. As we shall show in this report, the implementation of a wide FOV laser may be such an application. In the following sections, the basic design and fabrication approaches for holographic lenses are described.

3.2 Design and Fabrication Approaches

A holographic lens can be fabricated with one of three basic approaches. It can be recorded interferometrically using optical fields generated with conventional optics, interferometrically using optical fields generated with computer-generated hologram(s) or directly as a computer-generated hologram in the form of a kinoform. The features of these three main fabrication approaches are described below.

3.2.1 Interferometrically Formed Holographic Optical Element

When an optical field $F(x,y)$ interferes with another field described by $G(x,y)$, the resulting intensity pattern is equal to

$$|F + G|^2 = |F|^2 + |G|^2 + F^*G + FG^*. \qquad (1)$$

Recording the pattern on a thick recording material to form a volume Bragg hologram, the complex transmittance of the resulting holographic element can be confined to a single diffraction order, F^*G or FG^*. The realizability of a given phase function is dependent on the realizability of F and G.

The earliest holographic lens was fabricated by interfering a diverging beam with a collimated beam. The resulting hologram is essentially a lens with a spherical phase transmittance function. Such a holographic lens acts as a perfect (diffraction limited) collimating or focussing lens when used in the exact geometry of the recording system. However, it performs poorly as an imaging lens or a Fourier transform lens where it is necessary accommodate a range of input beam angles. As we shall show in Section 4, a holographic lens can provide good performance over a wider range of incident angles if the phase function is aspheric.

The optimum phase function for the diffractive lens for a particular application can be obtained analytically or numerically using a ray trace design program. However, it is difficult to generate accurately wavefronts other than spherical wavefronts with conventional optical components. The optimum phase function for a particular holographic lens can be quite arbitrary and it may not be possible to realize such phase functions interferometrically with wavefronts generated with conventional optics. On the other hand, with the mathematical description of the needed phase function, a computer-generated hologram can easily be fabricated to produce the desired phase function.

3.2.2 Computer-Generated Holograms and Kinoforms

Computer-generated holograms have typically been fabricated on photoresist, photographic film or plate in the form of a thin hologram. The maximum diffraction efficiency that can be achieved with absorptive recording material such as photographic film is only 6.25%. With a phase modulation material such as photoresist, the diffraction efficiency achievable is higher but it is still no more than 40.5%. Fabrication techology now permits a CGH to be fabricated in the form of a kinoform [1] which provides on-axis operation with close to 100% efficiency by using blazed fringe gooves. A kinoform diffractive lens can be fabricated with the so-called "binary optics" approach using multiple binary masks [2] or with diamond turning [3]. Arbitrary phase functions can be realized with the binary optics approach while the diamond turning technique is limited to the fabrication of circularly symmetric optical elements. However, the highest spatial frequency that can be implemented with either technique is limited. The fastest kinoform lens that can be fabricated currently for 0.8μm operation is about f/2. Recall that the lens for the wide FOV laser receiver has an f/number of about f/0.7. The lens is therefore much too fast to be fabricated as a kinoform with current fabrication technology.

3.2.3 Computer-Originated Holographic Elements

An alternate fabrication approach pioneered by ERIM is to combine computer-generated hologram with the interferometric fabrication technique by interfering wavefronts produced by two CGHs, or by interfering a wavefront generated with conventional optics with one produced by a CGH. This hybrid approach permits very fast lens (f/number <1 at $0.8\mu m$) with arbitrary phase function to be fabricated. An element fabricated by such a technique is often referred to as a Computer-Originated-Holographic-Optical-Element (COHOE) [4]. The general procedure for fabricating a fast aspheric COHOE lens is as follows.

After the desired phase function $\theta(x,y)$ is obtained, it is matched to the closest spherical function $S(x,y)$. The spherical phase function which contains most of the optical power needed for the diffractive lens can be introduced accurately with a diverging or converging beam as shown in Figure 3. The remaining aspheric term, $\theta(x,y)$-$S(x,y)$ (or its conjugate), is then encoded in the CGH. With most of the optical power provided by the spherical recording beam, the fabrication of the CGH becomes much less demanding. Aspheric diffractive lenses as fast as f/0.5 at $0.8\mu m$ can be fabricated using such a hybrid approach.

3.2.4 Diffraction Efficiency and Bragg Conditions

To achieve high diffraction efficiency, the holographic lens must operate in the volume Bragg diffraction regime which necessitates the use of a high spatial carrier. To be able to operate as an on-axis lens, one approach is to combine two holograms with the same spatial carrier, one being an off-axis lens and the other essentially a grating, as illustrated in Figure 4. When the two holograms are bonded together with the emulsion sides towards each other, the resulting holographic lens behaves as an on-axis lens.

Computer-Originated Hologram

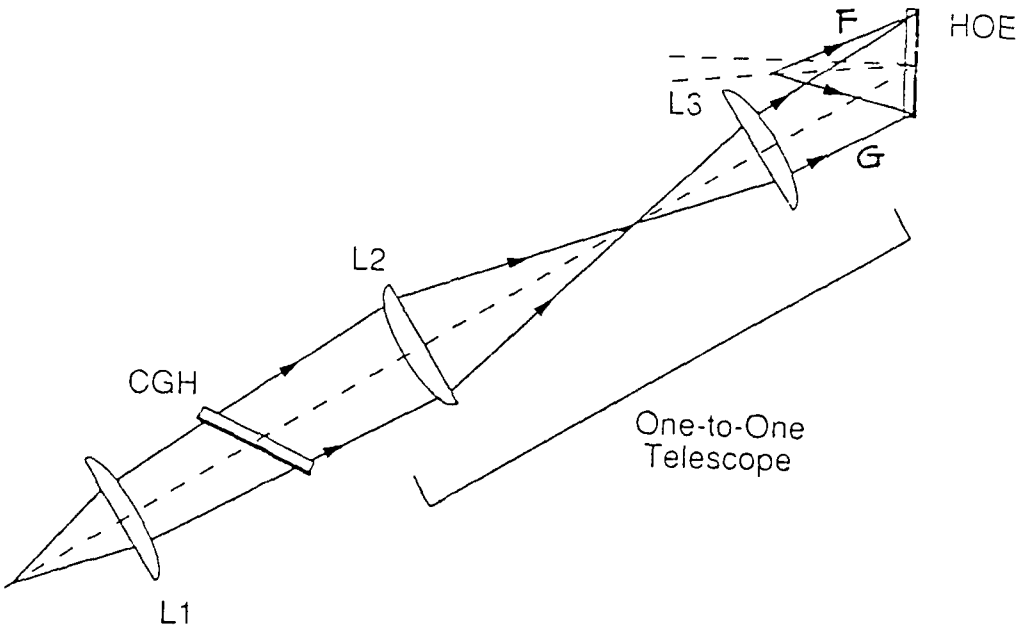

Figure 3. Fabrication of Computer-Originated Holographic Optical Element (COHOE).

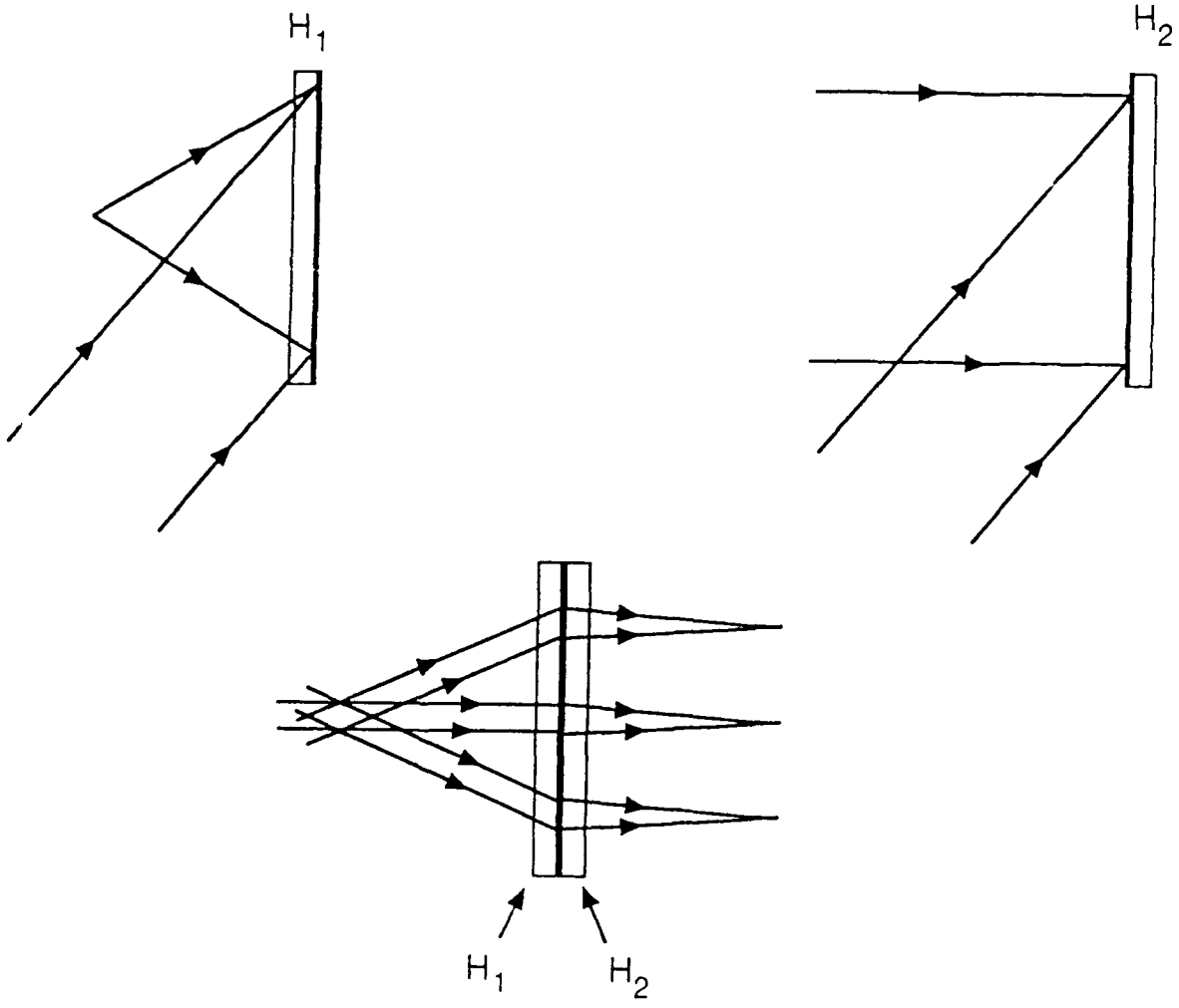

Figure 4. Fabrication of on-axis holographic lens with two off-axis volume Bragg holograms.

Another design consideration is that the fringe formation in the hologram must not only provide the desired phase function, it must also satisfy the Bragg condition. To satisfy the Bragg condition over all input field angles, one of the constructing beams must match the playback geometry. For example, if the hologram is to be used as a Fourier transform lens, a suitable geometry is shown in Figure 5(a). To assure uniform diffraction efficiency over all input angles, one the constructing beams for the hologram must be a diverging beam originating from the center of the input aperture as illustrated in Figure 5(b). With such a recording geometry, the principal ray for an incident beam at any angle within the FOV will satisfy the Bragg condition perfectly, resulting in near 100% diffraction efficiency. The diffraction efficiencies taper off from the center as the rays incident on the holographic lens become more and more off-Bragg. The angular bandwidth of Bragg diffraction thus limits the effective f/number of the lens but no restriction is placed on the FOV that can be achieved. We should note that the sandwiched holographic lens is angularly selective only in the direction of the carrier. In the direction perpendicular to the carrier grating vector, the input plane wave that passed through the input aperture is diffracted with uniform efficiency. The restriction on the effective f/number of the lens due to Bragg angular selectivity therefore occurs only along one dimension.

To determine the smaller effective f/number that can be practically achieved, we analyzed the diffraction efficiencies across the sandwiched holographic lens for various input beam angles using the multi-wave formulation [5]. (It is a more rigorous and precise formulation for the analysis of Bragg diffraction than Kogelniks' well known coupled-wave formulation [6]). In the analysis, the refractive index modulation (Δn) of the recording material was limited to 0.05 which can be readily obtained using dichromated gelatin. Assuming an emulsion thickness of 7μm, the computed diffraction efficiencies in the direction of the carrier across the holographic lens for input beam

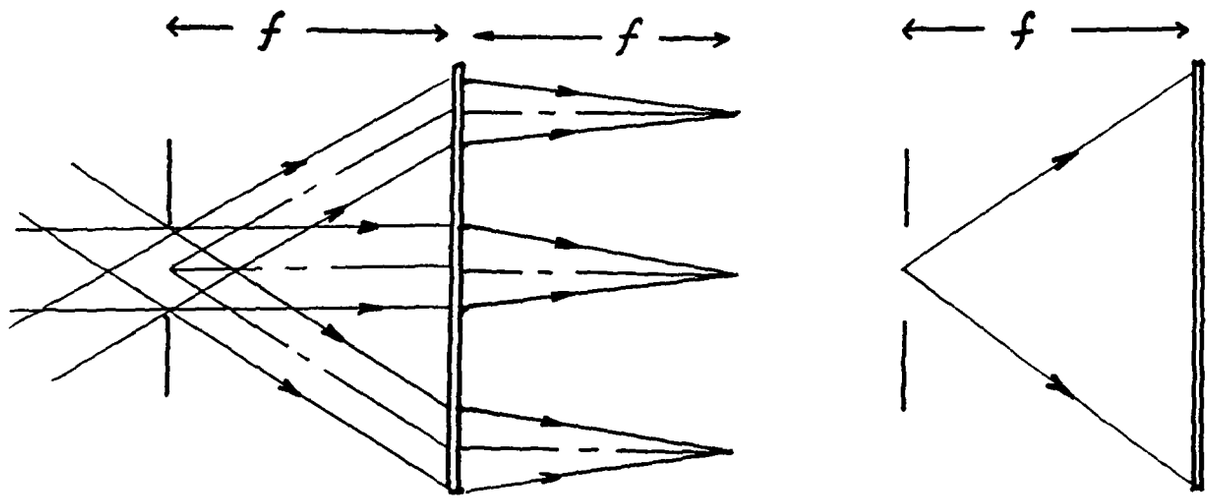

(a) Playback Geometry

(b) One of the Recording Beams.

Figure 5. Matching one of the recording beams to the playback geometry. (a) Playback geometry, (b) recording beam.

angles of -20°, 0° and 20° are shown in Figure 6(a), (b) and (c). The diffraction efficiency is uniformly high for the three incident angles with the peak efficiency averaging about 90%. However, diffraction occurs only over a width of 5mm of the lens. With a focal length of 12mm, a 5mm diameter restricting aperture results in an effective f/number of f/2.4. Due to the restriction imposed by the angular selectivity of Bragg diffraction on the f/number of the holographic lens, the lens will be designed to provide the needed focussing performance at f/2.4.

With the diffraction efficiency dropping down to zero at the edge of the circular aperture along one dimension, not all the light that passes through the input aperture is diffracted and focussed onto the detector array. The system efficiency of the laser receiver obtained by integrating the curves in Figure 6 over a circular aperture is about 54%.

The hybrid or COHOE fabrication approach provides the ability to realize any legitimate phase function for the holographic lens without restricting its FOV. It was therefore selected as the fabrication approach for the wide FOV holographic lens. The design of the wide FOV is presented in the next section.

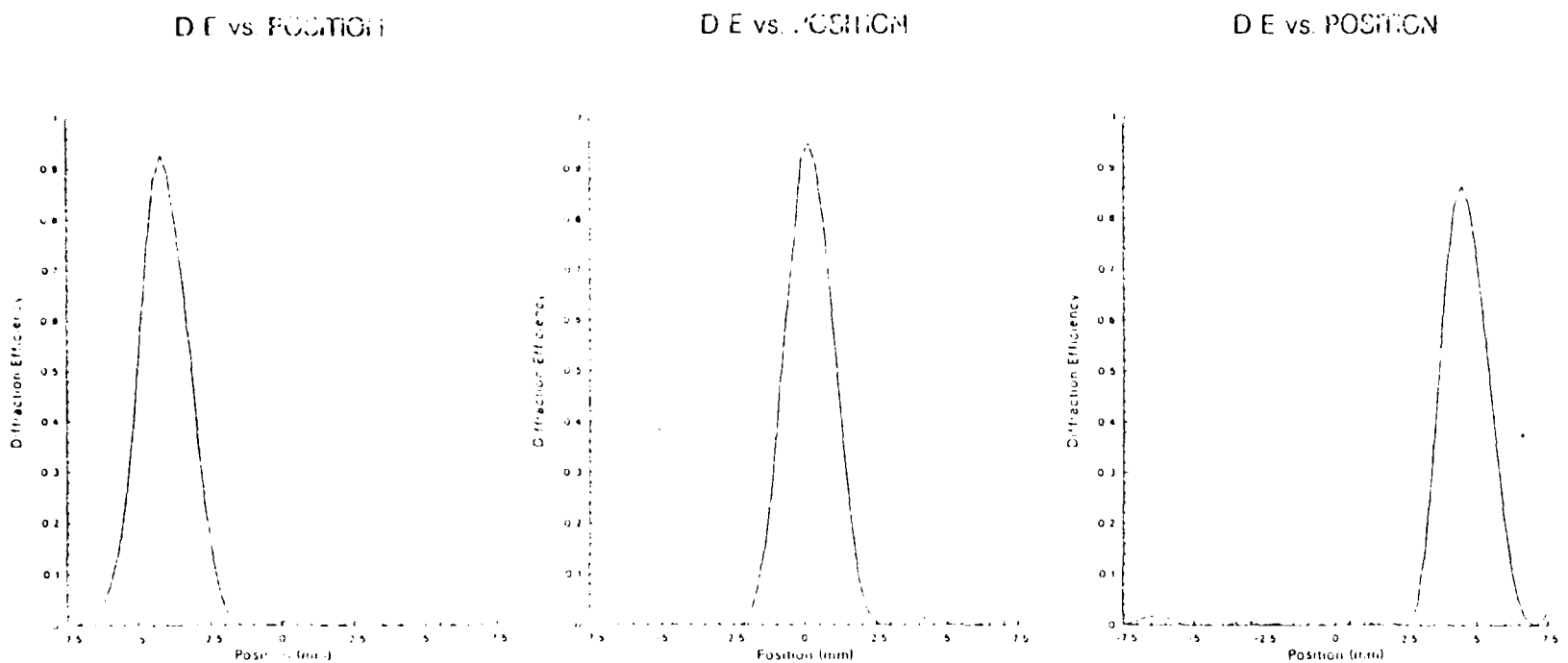

Figure 6. Diffraction efficiency as a function lens position for input angles of (a) $\theta_x = -20^o$, (b) $\theta_x = 0^o$ and (c) $\theta_x = 20^o$

This page intentionally left blank.

4.0 DESIGN OF WIDE FOV HOLOGRAPHIC LENS

In this section the design of the holographic lens is described and its imaging performance is analysed. A system geometry as illustrated in Figure 7 was chosen for the imaging system. This Fourier transform system geometry was chosen because: 1) it simplifies analysis, 2) it has been shown to be the optimum imaging geometry for wide angle operation [3] and, 3) it minimizes the size of the window required on the surface of the aircraft.

As stated in the previous sections, the desired phase function for the holographic lens is one that produces a symmetric focussed spot with a constant spot diameter at f/2.4 somewhere between 15μm and 30μm over a FOV of $\pm 26.7^{\circ}$. It is well known that a parabolic phase function produces a flat image plane over a fairly wide FOV and it therefore provides a good starting point for the design of the holographic lens. A parabolic phase function is described by

$$\phi = -\frac{\pi}{\lambda f}(x^2 + y^2) \tag{2}$$

where λ is the operating wavelength and f is the focal length of the lens. The dominant aberration introduced by a parabolic phase function, particularly near on-axis, is spherical aberration. Comparing with a Gaussian sphere, the spherical aberration term can be written as [7]

$$S_1 = \frac{f}{16(f\#)^4} \tag{3}$$

where f# is the f/number of the lens (focal length/diameter of lens aperture). The maximum spot diameter at the paraxial focal plane can be approximated as

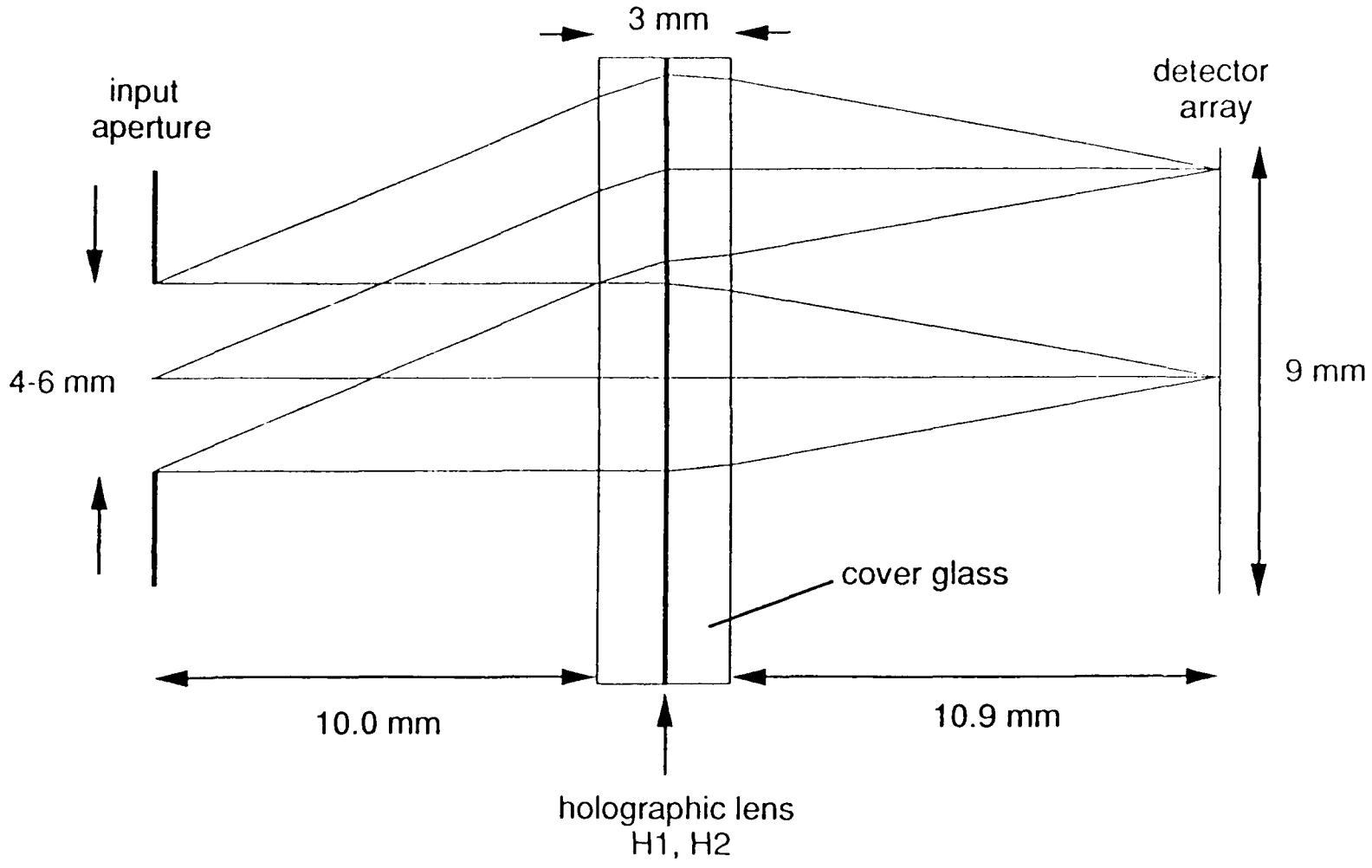

Figure 7. Geometry of wide angle holographic lens.

$$D = \frac{2f}{16(f\#)^3} \qquad (4)$$

The dominant aberration is spherical for all field angles and the spot diameter remains constant over a fairly wide angle. At the more extreme angles, however, coma also becomes significant. In Figure 8, we show the spot diagrams obtained by ray tracing for three input field angles for a f/2.4 lens having a parabolic phase function. The focussed spot begins to show significant coma and the spot diameter grows significantly at 22.5°. In this report, the focussed spot size will be defined by the root-mean-squared (rms) spot diameter. In Figure 9, the rms spot diameter is plotted against input field angles for a lens with an f/number of f/3, f/2.4 and f/2. We see that the focussed spot remains fairly constant and small over the ±26.7° FOV at f/3. When the aperture is increased to f/2.4, however, the spot diameter grows significantly for field angles over 18°. Although the parabolic phase function appeared to provide adequate performance for a f/3 lens, we looked into means to improve lens performance to allow the lens to operate satisfactorily at f/2.4, the limit imposed by the angular selectivity of Bragg diffraction.

Before attempting to derive a phase function that can provide the needed focussing performance with a larger numerical aperture, the effects other parameters have on system performance were analyzed such that they can be accounted for in the optimization. Because the focal length of the lens was so short (12mm), a significant parameter is the thickness of the flat glass substrates which together occupied about 3.2mm. As described in Section 3, the on-axis holographic lens was formed by bonding two off-axis holograms together, emulsion sides against each other. (The bonding also sealed the emulsions against degradation by moisture and scratches). We analyzed the performance of the parabolic holographic lens with the presence of the glass substrates which are required to support the emulsions. In Figure 10,

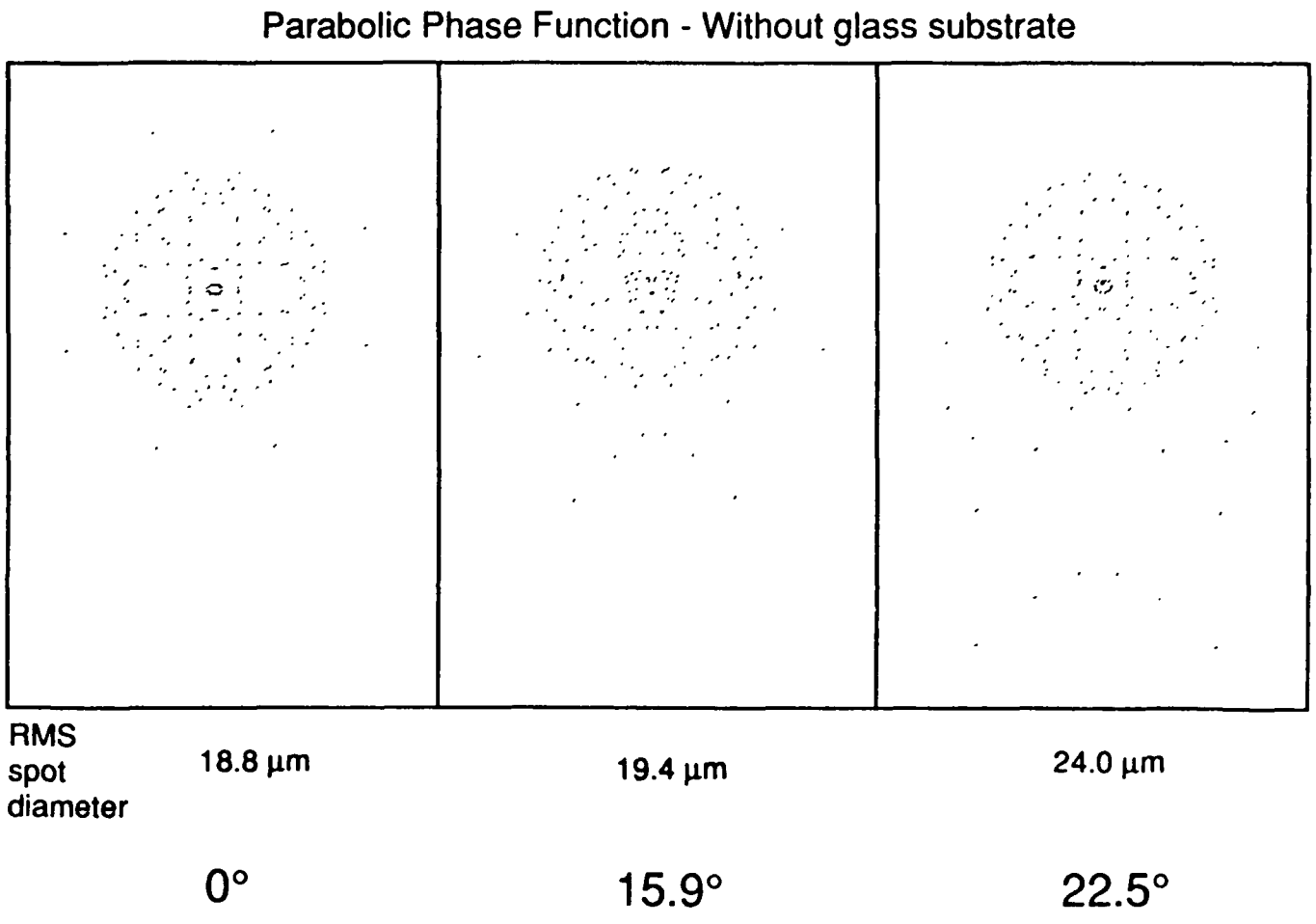

Figure 8. Spot diagrams of focussed spot obtained with parabolic phase function for input angles of 0^{o}, 15.9^{o} and 22.5^{o}.

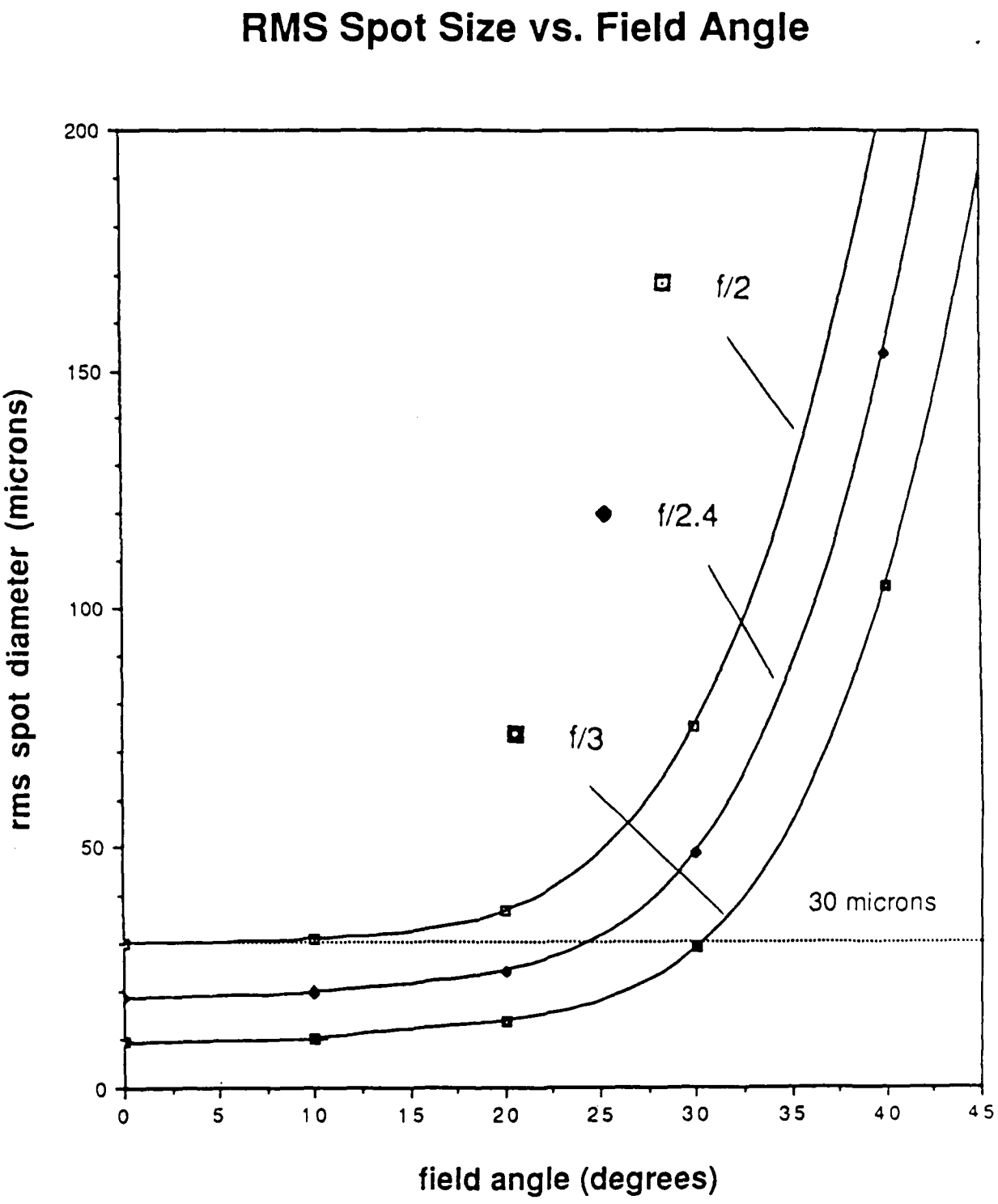

Figure 9. RMS spot size as a function of field angles for a parabolic phase function.

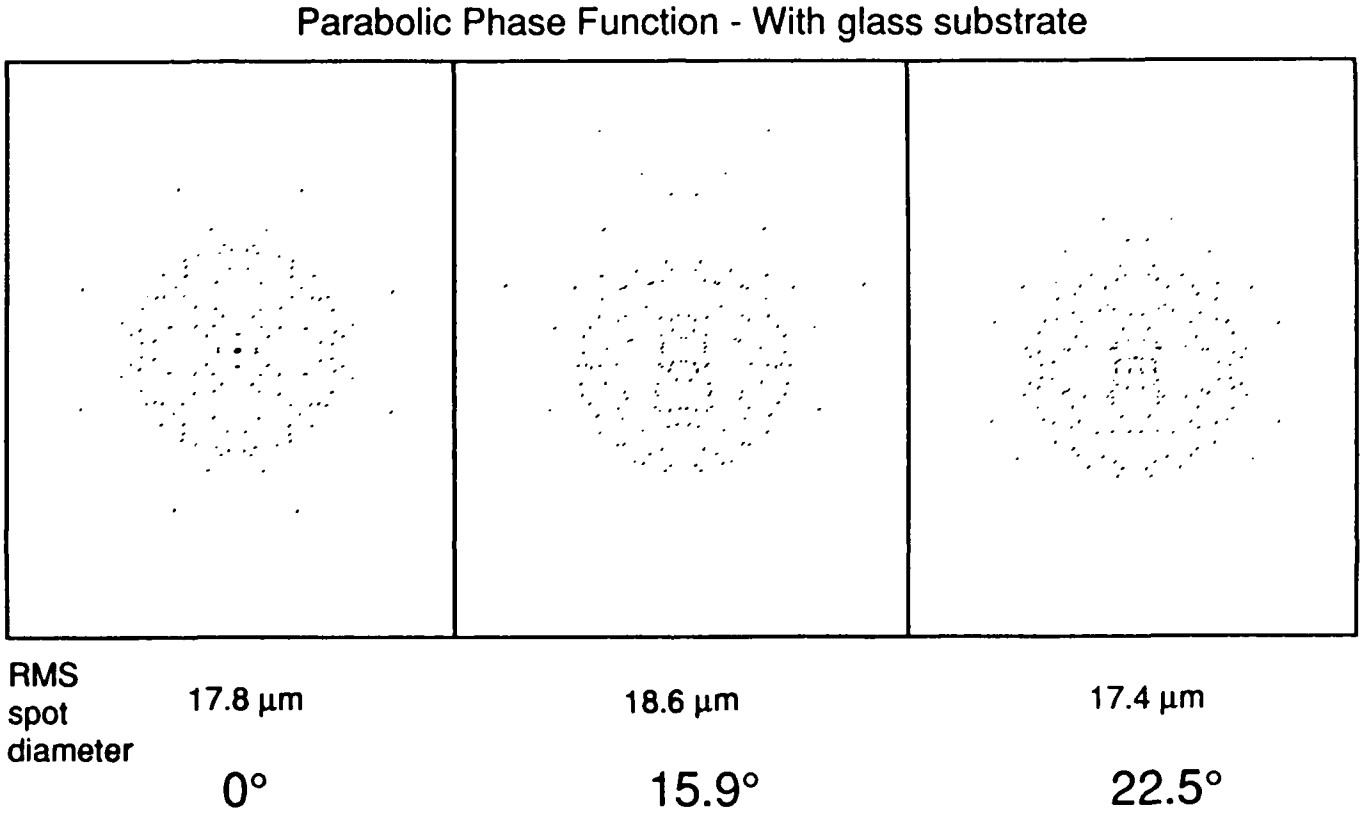

Figure 10. Spot diagrams of focussed spot obtained with parabolic phase function and glass substrates on both sides of the lens for input angles of 0^{o}, 15.9^{o} and 22.5^{o}.

we show the spot diagrams with the thickness of the glass substrates included. To our pleasant surprise, the focussed spots became more symmetric and uniformly smaller over the entire FOV. For comparison, we show in Figure 11 the rms spot size for a f/2.4 lens with a parabolic phase function with and without the glass substrates. With the glass substrates, the focussed spot maintained a constant spot diameter of $\simeq 20\mu m$ over a FOV of $\pm 32^{\circ}$ which is more than adequate to satisfy the requirement of the wide FOV laser receiver.

Analyzing further this interesting phenomenom, we found that the glass substrates on the two sides of the emulsion both played a role in reducing the aberrations of the imaging system. As shown in Figure 7, the holographic lens was located between the two glass substrates. We analysed the effects of each of the glass thicknesses separately and found that the presence of the glass at the input side reduced the off-axis coma while the glass at the output side reduced the spherical aberration for all field angles.

First we looked at the effect of the output converging beam propagating through the thickness of the glass substrate. It introduces spherical aberration which is given by [7]

$$S_1 = - \frac{(n^2-1)}{n^3} \frac{\Delta}{16(f\#)^4} \qquad (5)$$

where n is the refractive index of the glass substrate and Δ is the glass thickness. We see that the spherical aberration produced by propagating a converging beam through the thickness of the glass is of an opposite sign to that produced by the parabolic phase function. The amount of spherical aberration is reduced with increasing glass thickness but can never be completely removed. This can be seen by comparing Equations (3) and (5). The spherical aberration is eliminated when

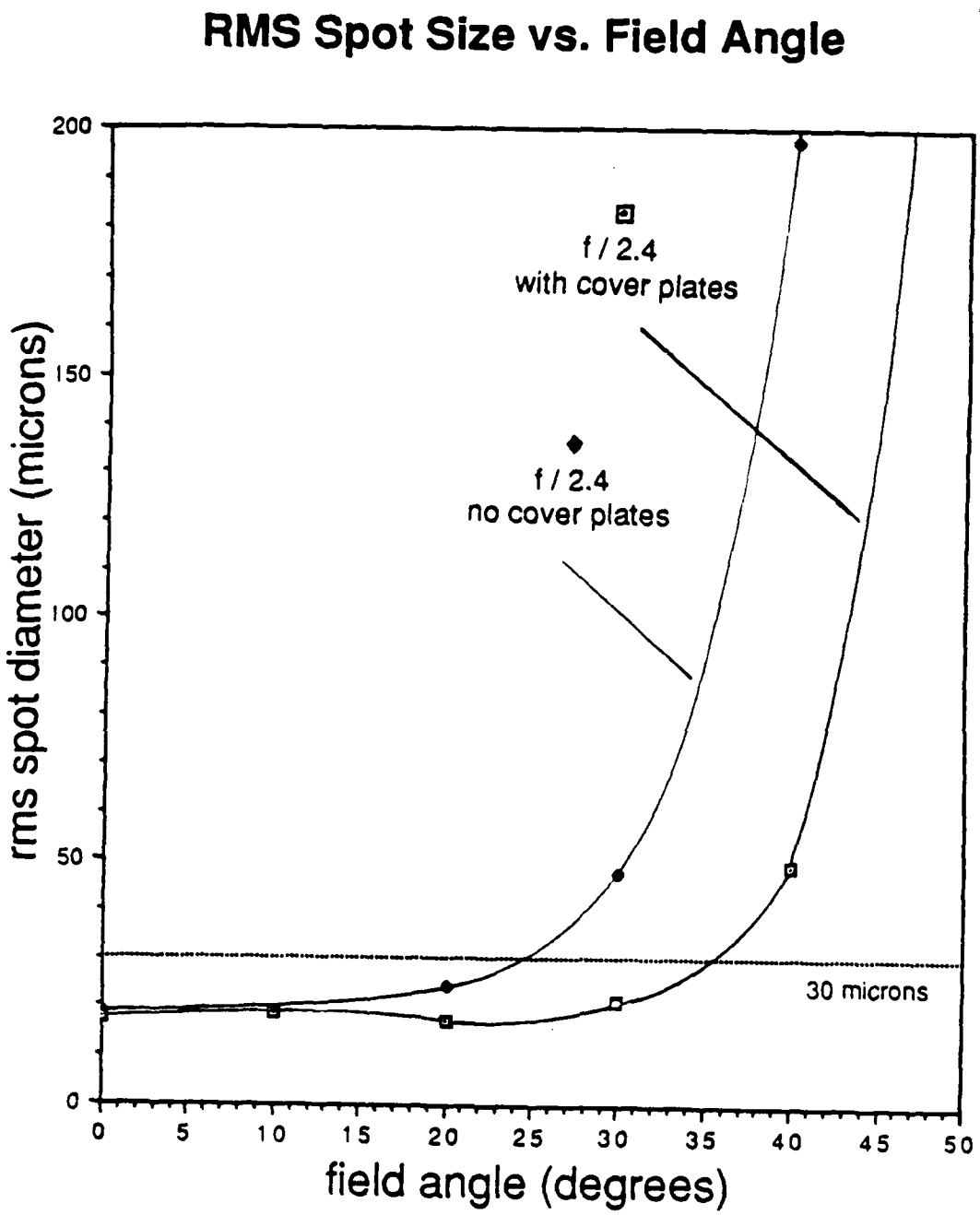

Figure 11. RMS spot size as a function of field angles for a parabolic phase function with glass substrate on both sides of the lens.

$$\Delta = \frac{n^3}{n^2 - 1} f \qquad (6)$$

which for n=1.5, requires that $\Delta=2.7f$. Since $\Delta \leq f$, the complete removal of the spherical aberration with glass thickness is impossible. Furthermore, since light weight is one of the reasons for selecting the holographic approach, the use of a glass substrate thicker than that required to maintain rigidity and flatness cannot be justified. To more fully remove the spherical aberration, a corrector plate (a negative lens with the appropriate phase function) can be added at the input aperture. However, as noted before, the design goal is not to produce a near diffraction-limited spot ($\simeq$2.5μm spot diameter) but to produce a constant spot size 15 to 30μm in diameter over the FOV. Moreover, the use of a corrector plate at the input aperture could place additional constraints on the conformality of the window or the type of window material that can be used. It was therefore decided that further reduction of spherical aberration was not warranted.

The glass substrate at the input side also helps in reducing the overall aberration, particularly off-axis coma. The parabolic phase function has a slope that is too steep near the edge of the lens to provide optimum off-axis performance. An incident plane wave at angle θ propagating through the thickness of the glass is shifted closer to the center of the lens by an amount of

$$L(\theta) = \Delta \tan\left[\sin^{-1}\left(\frac{\sin\theta}{n}\right)\right] \qquad (7)$$

This θ dependent shift in the aperture stop effectively reduces the non-spherical aberrations [7] and produces a focussed spot that was fairly symmetric as shown in Figure 10.

The analysis to determine the effects of glass substrates on system performance thus evolved into a solution to the design problem. It was determined that the needed lens performance over the entire FOV can be satisfied with a parabolic phase function and glass substrates on both sides of the emulsion. In the following section, the fabrication approach taken to implement the design of the holographic lens is described.

5.0 FABRICATION OF WIDE FOV HOLOGRAPHIC LENS

The holographic lens can be fabricated as described in Section 3 if it can be recorded at the same wavelength as the operating wavelength of the laser receiver. Recording at 850nm, the first hologram is fabricated by simply interfering an off-axis reference plane wave with a diverging beam from a point source located at the center of the input aperture, one focal length in front of the hologram as shown earlier in Figure 4. The spherical beam provides the appropriate optical power and also ensures the principal ray passing through the input aperture at any angle satisfies the Bragg condition. The resulting hologram is essentially an off-axis zone plate. The phase correction is placed in the second hologram by interfering an identical off-axis reference plane wave with an optical field carrying the phase function $\phi(x,y) = \theta(x,y) - S(x,y)$ where

$$\theta(x,y) = -\frac{\pi}{\lambda f}(x^2 + y^2) \tag{8}$$

is the desired parabolic phase function and

$$S(x,y) = \frac{2\pi}{\lambda}\left[f\sqrt{1 + \left[\frac{x^2 + y^2}{f^2}\right]}\right] \tag{9}$$

is the spherical phase function of the diverging beam. In the equations, f denotes the focal length of the lens and λ = 850nm is the operating wavelength of the laser receiver. Available holographic materials, however, are completely insensitive to radiation at such a long wavelength. The holographic lens must therefore be recorded at a shorter wavelength where recording materials such as dichromated gelatin and photopolymer provide adequate sensitivity.

In the fabrication of the wide FOV holographic lens, the 488nm line of an Ar^+ laser was used for the holographic recording. The large wavelength shift between recording and playback must be taken into account in the design. Ideally, the recording geometries and wavefronts used to record the two holograms at 488nm should produce holograms that are identical to those obtained with 850nm laser recording beams as described above. However, it is not necessary to have a perfect match in Bragg angles. The finite angular bandwidth of Bragg diffraction permitts the system to tolerate small deviations from the ideal Bragg angles. This is an important design consideration because to match the phase function and the Bragg angles exactly, both recording beams at 488nm for both holograms must be non-spherical wavefronts that can only be produced with computer-generated holograms (CGHs). But if the holographic lens is to match the desired phase function exactly and the Bragg angles only approximately, then at least one of the two recording beams can be a simple spherical wavefront. The use of a spherical recording beam not only simplified the fabrication, it was imperative for the wide FOV holographic lens because the optical power of the lens was so strong that it can only be derived from a diverging spherical beam.

5.1 Fabrication of H_1 in Sandwiched Holographic Lens

The sandwiched holographic lens was composed of two holograms, the first hologram H_1 provides the spherical phase function with the needed optical power and the second hologram H_2, the aspheric terms. When recording at 488nm, the design strategy was to produce H_1 using only spherical beams and all the phase corrections, including those due to the wavelength shift, were put into H_2.

To fabricate hologram H_1, the positions of the two recording point sources at 488nm can be determined by solving the following equations [8] for (R_o, α_o) and (R_r and α_r) as defined in Figure 12 where $R_i=f$, $\alpha_i=0$, $R_k=\infty$, $\alpha_k=45^\circ$, $\lambda_c=488$nm and $\lambda_p=850$nm.

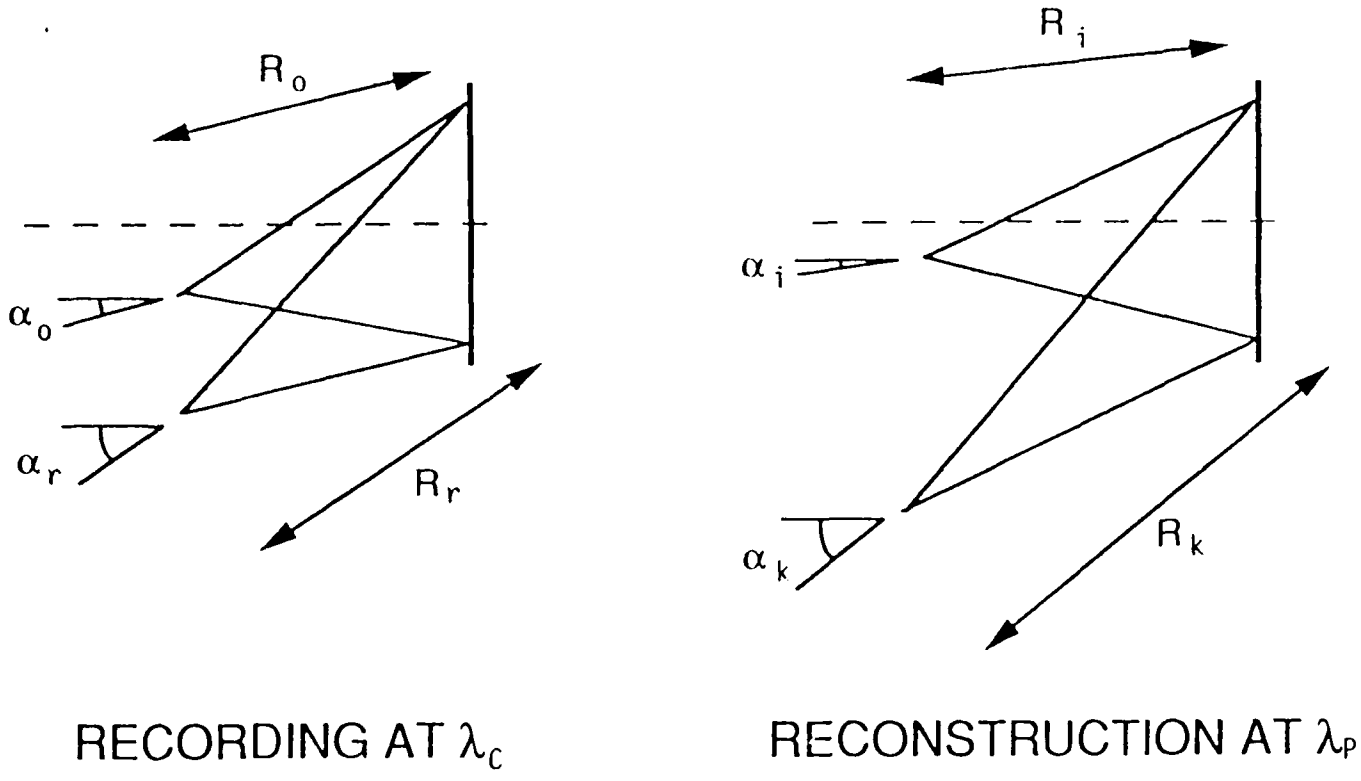

Figure 12. The determination of point source locations for recording that compensate for wavelength shift between recording and playback.

$$\frac{1}{R_r} = \frac{1}{2\mu}\left(\frac{\mu+1}{R_i} + \frac{\mu-1}{R_k}\right)$$

$$\frac{1}{R_o} = \frac{1}{2\mu}\left(\frac{\mu-1}{R_i} + \frac{\mu+1}{R_k}\right)$$

$$\sin\alpha_r = \frac{1}{2\mu}\left[(\mu+1)\sin\alpha_i + (\mu-1)\sin\alpha_k\right]$$

$$\sin\alpha_o = \frac{1}{2\mu}\left[(\mu-1)\sin\alpha_i + (\mu+1)\sin\alpha_k\right] \qquad (10)$$

where

$$\mu = \frac{\lambda_p}{\lambda_c} \quad .$$

The desired diffraction order of the hologram recorded at 488nm can be described by

$$\phi_{H_1} = \frac{2\pi}{\lambda_c}\left[R_r\sqrt{1+\left(\frac{x^2+y^2+2xR_r\sin\alpha_r}{R_r^2}\right)} + R_o\sqrt{1+\left(\frac{x^2+y^2+2xR_o\sin\alpha_o}{R_o^2}\right)}\right]. \qquad (11)$$

Not only must the thickness of the glass substrates be taken into account in the analysis of the lens performance, it must also be taken into account in the fabrication process. In the description above, the spherical wavefronts were assumed to reach the emulsion directly as shown in Figure 13(a). But in the sandwiched geometry, the emulsion of hologram H_1 is at the backside of the glass substrate. The diverging spherical waves must therefore propagate through the glass substrate to reach the emulsion as shown in Figure 13(b). However, propagating the spherical wavefronts through the finite thickness of the glass would introduce aspherical terms in the recorded phase function that had not been accounted for in the design. One way to circumvent the problem is to use converging spherical beams to illuminate the holographic plate from the emulsion side as shown in Figure 13(c). This would require

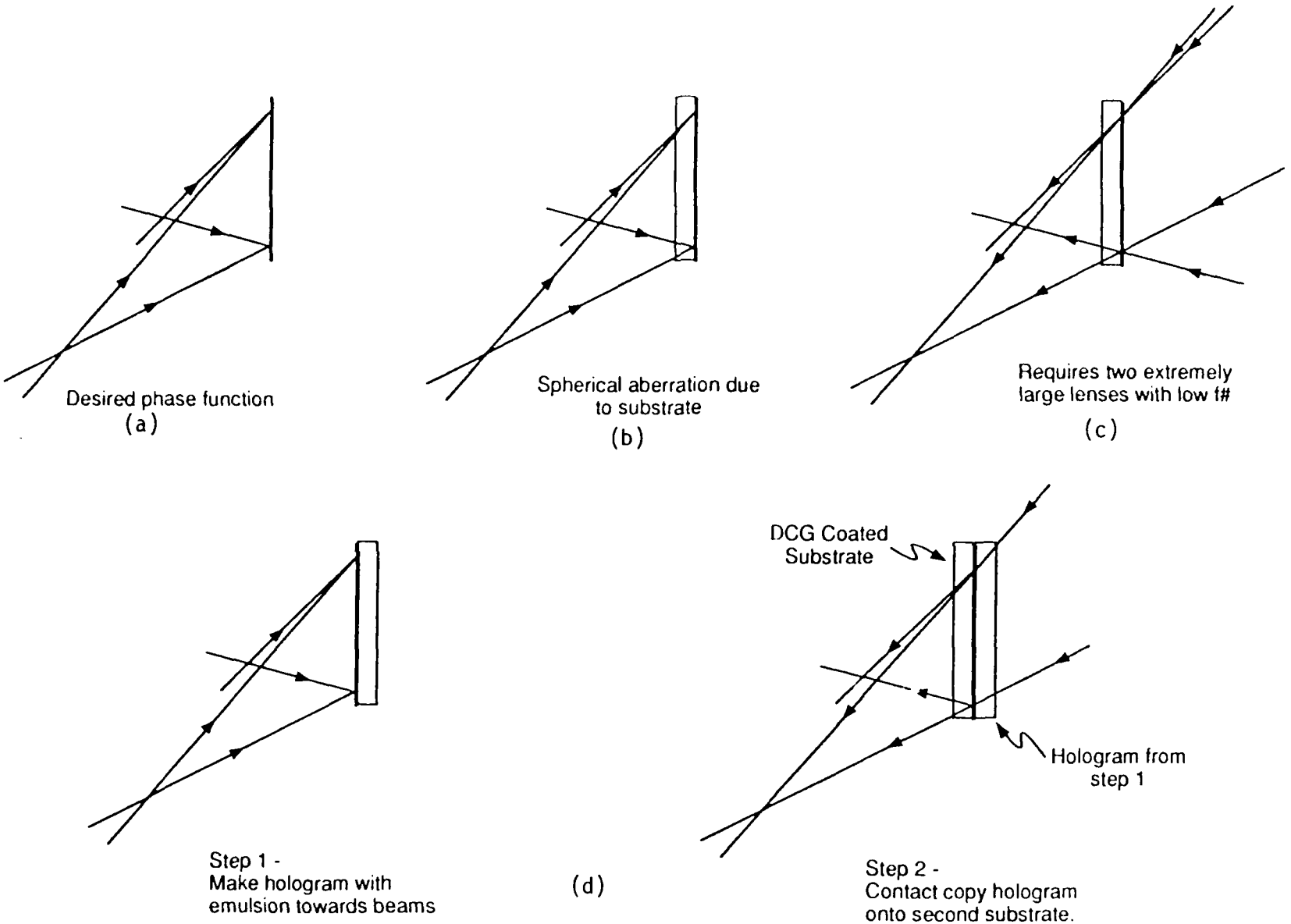

Figure 13. Fabrication geometry for hologram H_1 that avoids aberration caused by glass substrates.

very fast diffraction limited focussing lenses with large physical apertures that are difficult to obtain.

An alternate approach that we used in the fabrication of H_1 is to record an intermediate hologram with diverging spherical beams directly on the emulsion side and to contact copy the hologram onto another holographic plate using a converging beam that matches the conjugate of one of the recording beams as shown in Figure 13(d). We note that the converging wavefront used in the contact copying does not have to be perfectly spherical since the contact copying process transfers the phase function directly from the intermediate hologram to H_1. The converging beam needs only to match the conjugate of the recording beam close enough that the Bragg angles are copied with adequate accuracy onto H_1. (Recall in Section 3 we pointed out that due to the finite angular bandwidth of Bragg diffraction, small deviations from the exact Bragg conditions do not have any significant effect on the system efficiency).

The recording geometries for H_1 and H_2 are illustrated in Figure 14. For H_1, the point sources were very close to the holographic recording plate and to each other. We had problem fitting the microscope objectives which were used to generate the spherical beams into the recording geometry. To solve the problem, a holographic lens was constructed and used to generate one of the spherical beams as shown in Figure 15.

5.2 Fabrication of H_2 in Sandwiched Holographic Lens

To produce the desired parabolic phase function for 850nm operation, the second hologram H_2 should have a phase function of

$$\phi_{H_2} = -\frac{\pi}{\lambda_p f}(x^2 + y^2) - \phi_{H_1} . \qquad (12)$$

Recording Geometry

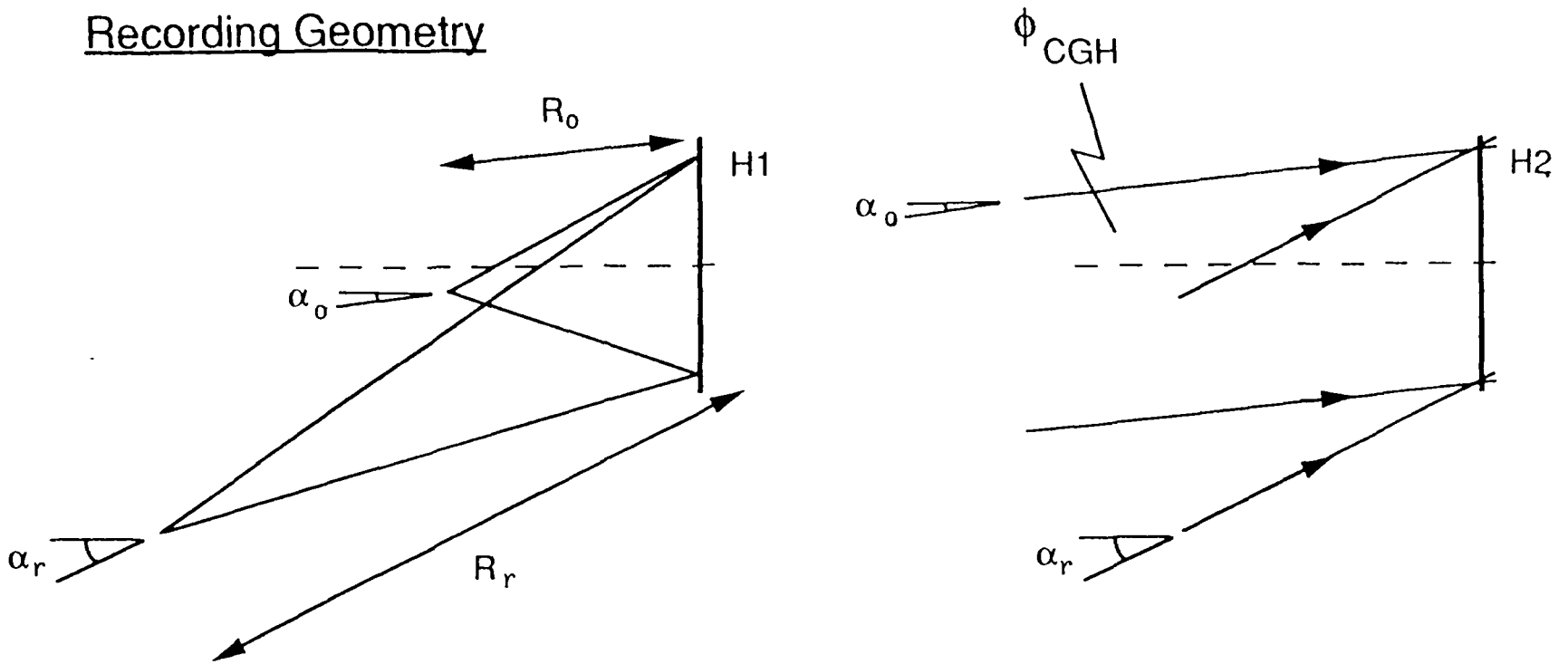

Design Parameters

$f = 12$ mm	$\lambda_C = 488$ nm	$R_r = 56.4$ mm	$\alpha_r = 33.8^\circ$
$\alpha_K = 45.0^\circ$	$\lambda_P = 850$ nm	$R_o = 15.2$ mm	$\alpha_o = 8.6^\circ$

Figure 14. Recording geometries for holograms H_1 and H_2.

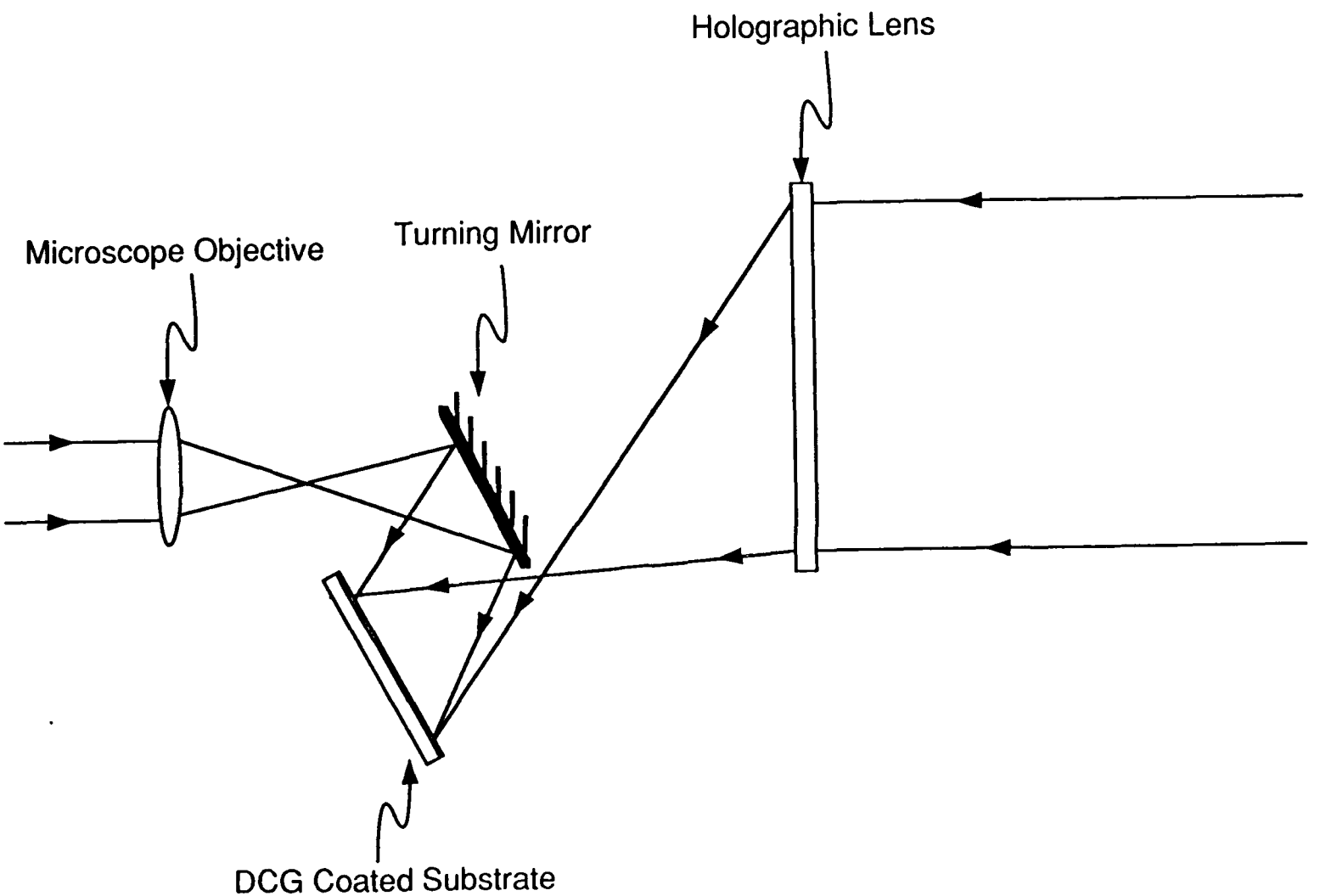

Figure 15. Optical arrangement for the fabrication of hologram H_1.

With ϕ_{H1} given in Eq. (11). In addition, H_2 must also satisfy the Bragg condition across the hologram. The appropriate positions of the point sources are again determined from Equation 10 where for H_1, $R_i=\infty$, $\alpha_i=0^\circ$, $R_k=\infty$ and $\alpha_k=45^\circ$. Since the angle of the reference beam for the two holograms is designed to match in order to create an on-axis lens, the angles of the recording beams α_o and α_r for H_2 were the same as those for H_1. For convenience, a plane wave was used as the off-axis reference beam (R_r, α_r) and all the phase corrections were placed in the object beam. The second hologram was made by interfering the wavefront from a CGH with the off-axis reference plane waves which added a $2\pi x \sin\alpha_r/\lambda_c$ phase term. The phase function of the object wave can be expressed as

$$\phi_{OBJ} = -\frac{\pi}{\lambda_p f}(x^2 + y^2) + \frac{2\pi}{\lambda_c} x \sin\alpha_r - \phi_{H_1} . \qquad (13)$$

Since the object wave itself was offset at an angle of α_o, the phase function to be generated by the CGH was therefore given by

$$\phi_{CGH} = \phi_{OBJ} - \frac{2\pi}{\lambda_c} x \sin\alpha_o , \qquad (14)$$

which can be shown to be equal to

$$\phi_{CGH} = -\frac{\pi}{\lambda_p f}(x^2 + y^2) + \frac{2\pi}{\lambda_p} x \sin\alpha_i - \phi_{H_1} \qquad (15)$$

where α_i is the common reference angle for both holograms at λ_p= 850nm.

The CGH was fabricated on film with a laser drum writer. To improve efficiency, it was contact copied onto photoresist on an optical flat. The CGH was fabricated at 3x scale and was imaged with a 3-to-1 reduction using a telescope onto the holographic plate. A

spatial filter was used at the spatial frequency plane to pass only the first order diffraction which contained the desired phase function. The recording setup for H_2 is shown in Figure 16. The use of a 3-to-1 reduction was necessary because the Modulation Transfer Function (MTF) of the laser writer was not wide enough to allow the phase function described in Equation 15 to be generated directly as a CGH.

The two holograms were both fabricated on dichromated gelatin, spin-coated on glass substrate with an emulsion thickness of about 7μm. Care was taken in the processing to ensure that no Bragg shift was introduced by swelling or shrinking of the emulsion. UV curing optical cement was then put on the emulsions and the two holograms were bonded together emulsion sides against each other. Before exposure to UV light, the bond remained in liquid form which permitted manipulation to align the holograms. The alignment was achieved by illuminating the entire lens with a plane wave at 850nm from the back side (i.e., the light propagated through the lens from what would normally be the focussing side). The light was focussed onto the CID detector array and the focus pattern was displayed on a TV monitor. The relative positions of the two holograms were then adjusted until the focus pattern became circularly symmetric. After the alignment was achieved, the sandwiched holograms were irradiated with UV light. The UV curing cement hardened and formed a solid bond which also sealed the holograms against environmental degradation. The hologram lens was then aligned with respect to the CID detector array and mounted permanently one focal length in front of the detector array and one focal length behind a 5mm circular aperture.

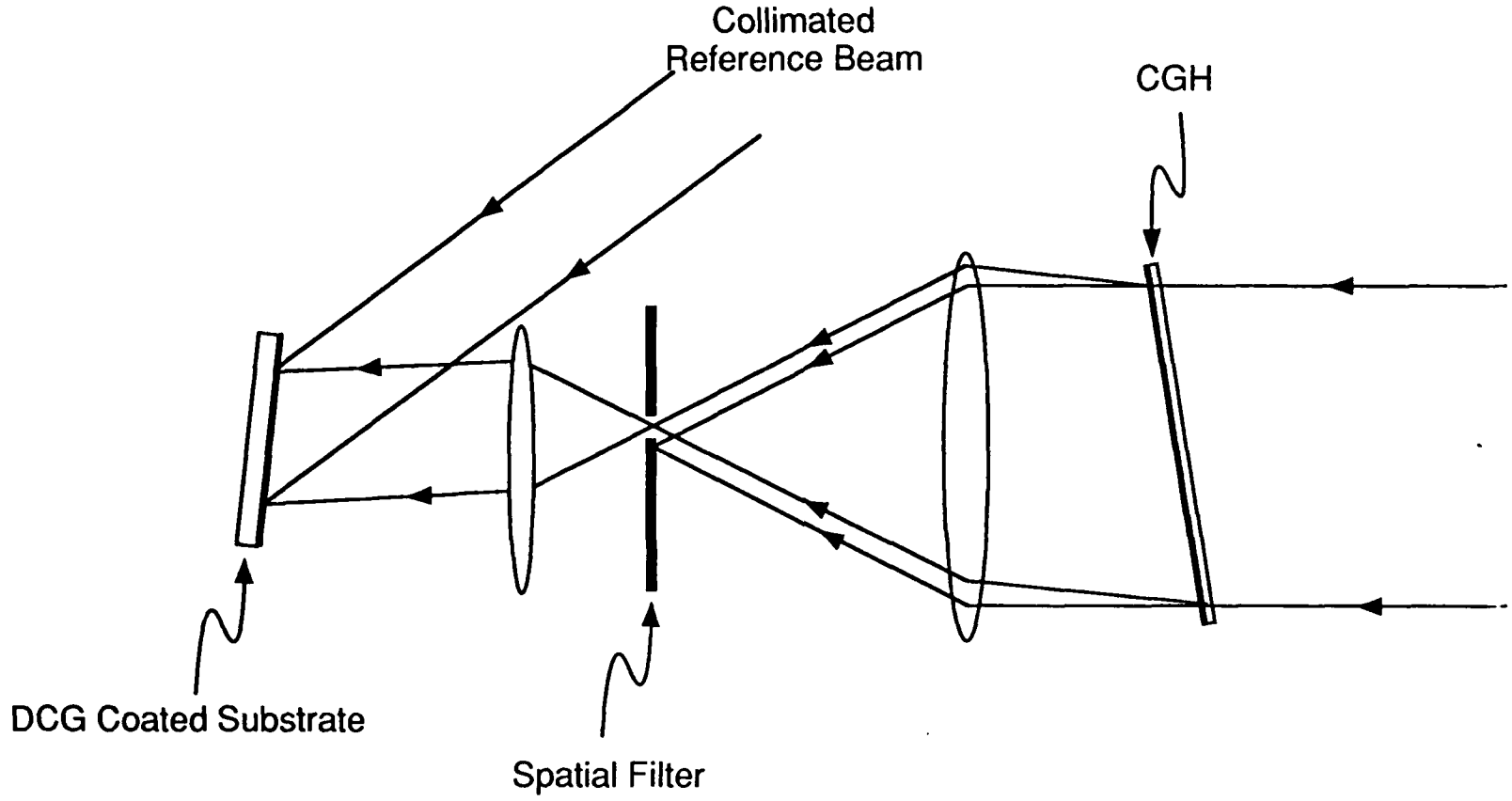

Figure 16. Optical arrangement for the fabrication of hologram H_2.

This page intentionally left blank.

6.0 EXPERIMENTAL RESULTS

The laser receiver was assembled and tested. A picture of the assembled unit is shown in Figure 17. As can be seen from the picture, the holographic lens occupies a minimum amount of space, leaving sufficient room to insert an E-O modulator for light level control or an atomic filter for background rejection on either side of the lens.

To test the performance of the wide FOV holographic lens, the laser receiver was mounted on a precision motorized rotator with the input aperture placed directly on the rotation axis. The input aperture of the laser was then illuminated by a laser diode emitting at 850nm. Different incident angles were obtained with high accuracy by rotating the laser receiver. The performance of the laser receiver was analysed by digitizing and recording the outputs of the CID camera with a video frame grabber and transfering the data to a computer.

One complication we encountered was that the output of the laser diode was highly astigmatic. To obtain a wavefront that was close to being a plane wave at the input aperture, the laser was moved far from the receiver (12 ft) and the laser light was made to diverge slightly by adjusting the collimating lens. This increased the size of the beam at the laser receiver and over the 5mm input aperture, the wavefront was close to being a plane wave.

The focussing performance of the holographic lens is shown in Figures 18(a) to (f) for incident angles of (θ_x=0°, θ_y=0°), (θ_x=-20°, θ_y=0°), (θ_x=20°, θ_y=0°), (θ_x=0°, θ_y=-15°), (θ_x=0°, θ_y=15°) and (θ_x=-15°, θ_y=15°). The focussed spot maintained a half-power width of about 2 pixels in both directions for all input angles. In Figure 19 and 20, pixel positions as determined by the locations of the peak values are plotted against incident angles in the x (horizontal) and y(vertical) directions respectively. The use of peak values to determine the spot

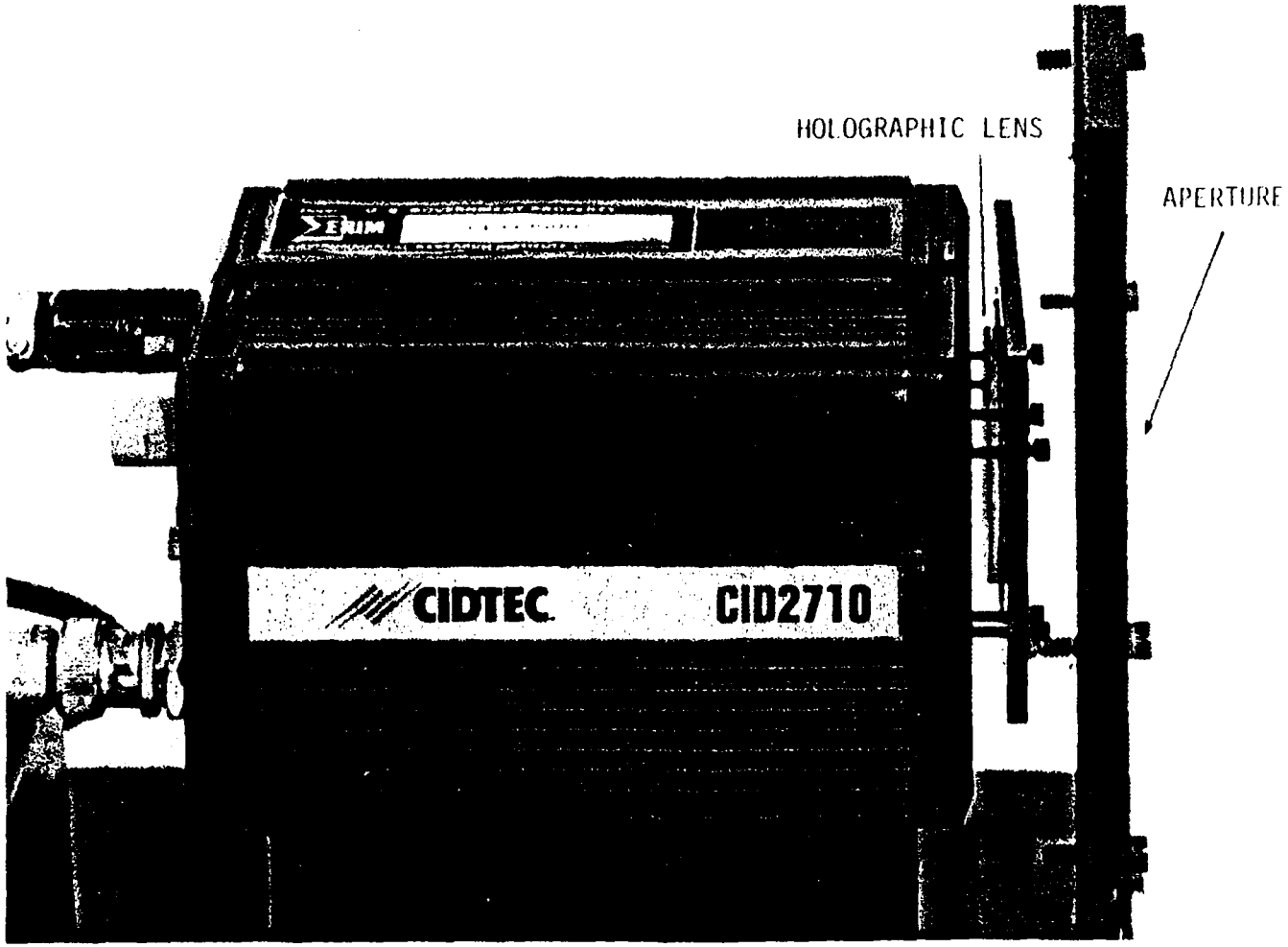

Figure 17. Holographic wide FOV laser receiver.

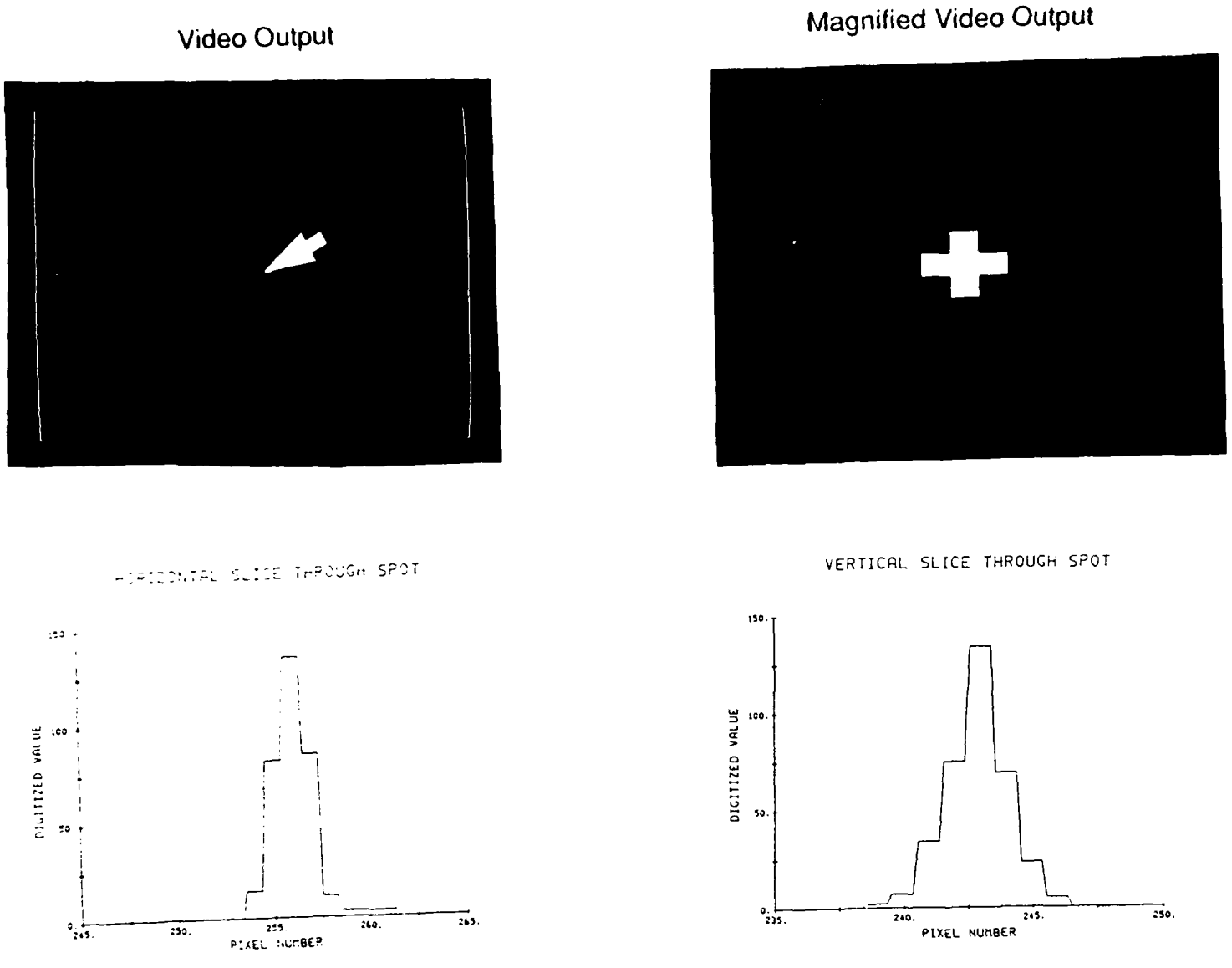

(a) Output of laser receiver for incident angles $\theta_x = 0°$ $\theta_y = 0°$

Figure 18. Focussing performance of holographic wide angle lens.

ERIM

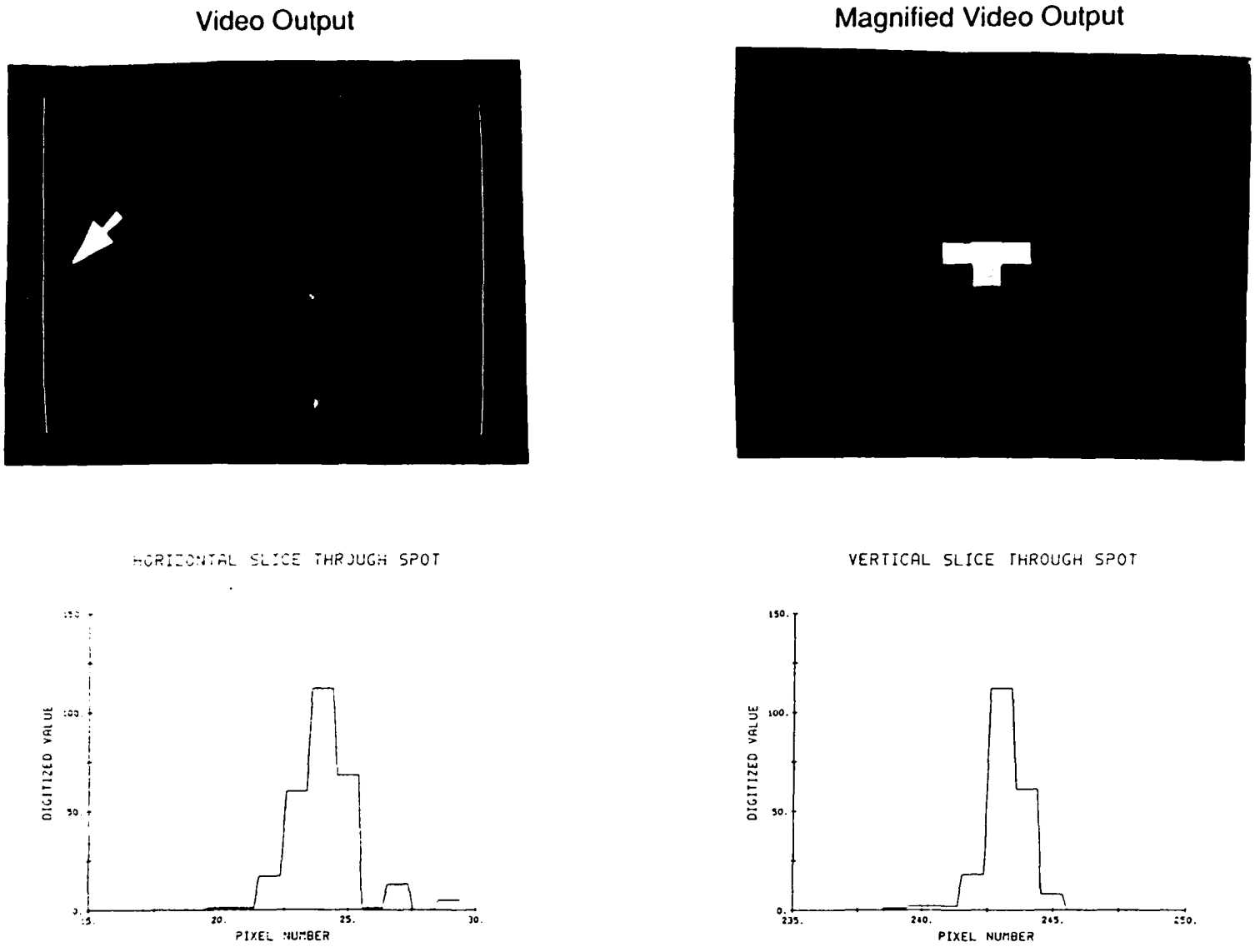

(b) Output of laser receiver for incident angles $\theta_x = -20°$ $\theta_y = 0°$

Figure 18. (Continued) Focussing performance of holographic wide angle lens.

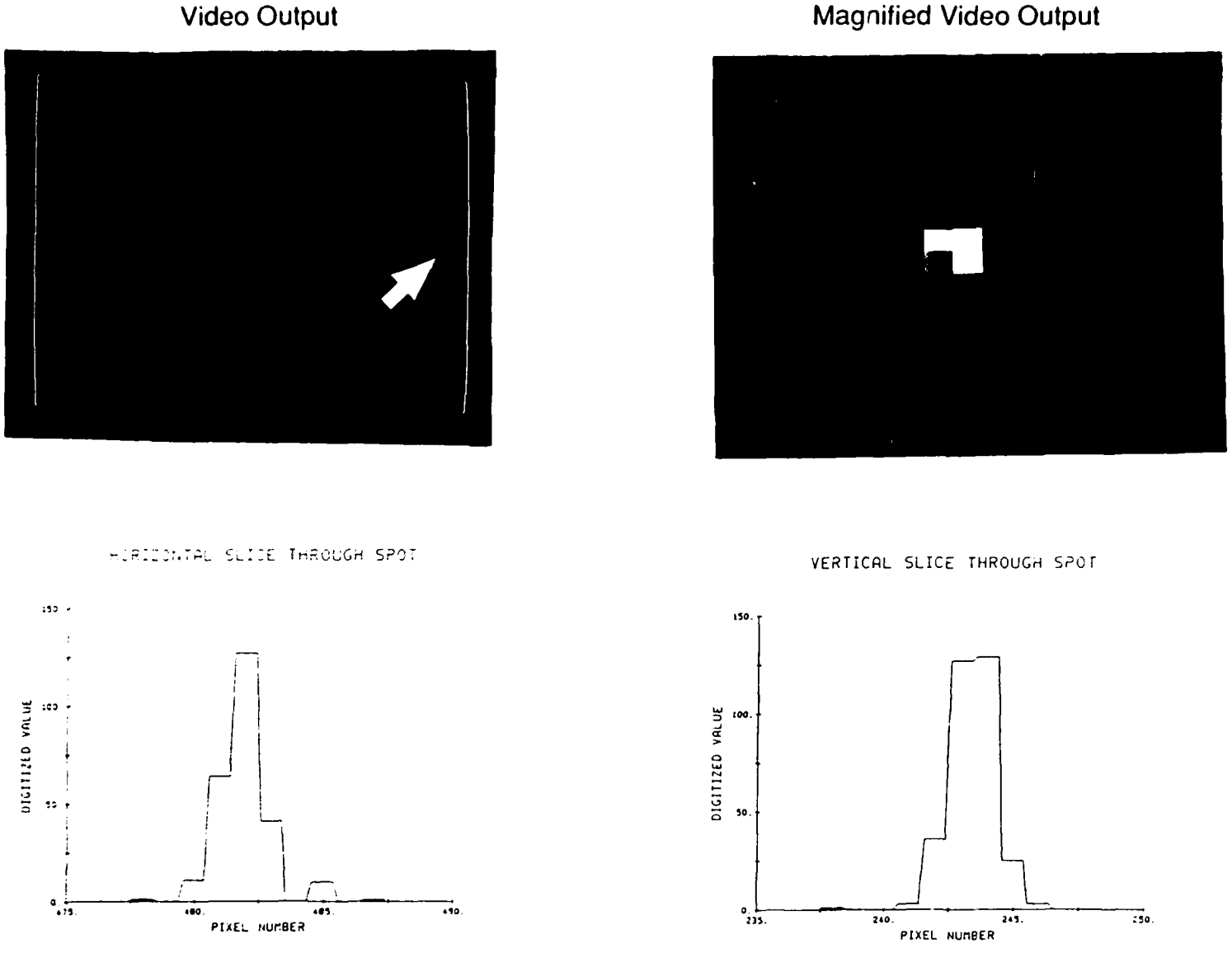

(c) Output of laser receiver for incident angles $\theta_x = 20°$ $\theta_y = 0°$

Figure 18. (Continued) Focussing performance of holographic wide angle lens.

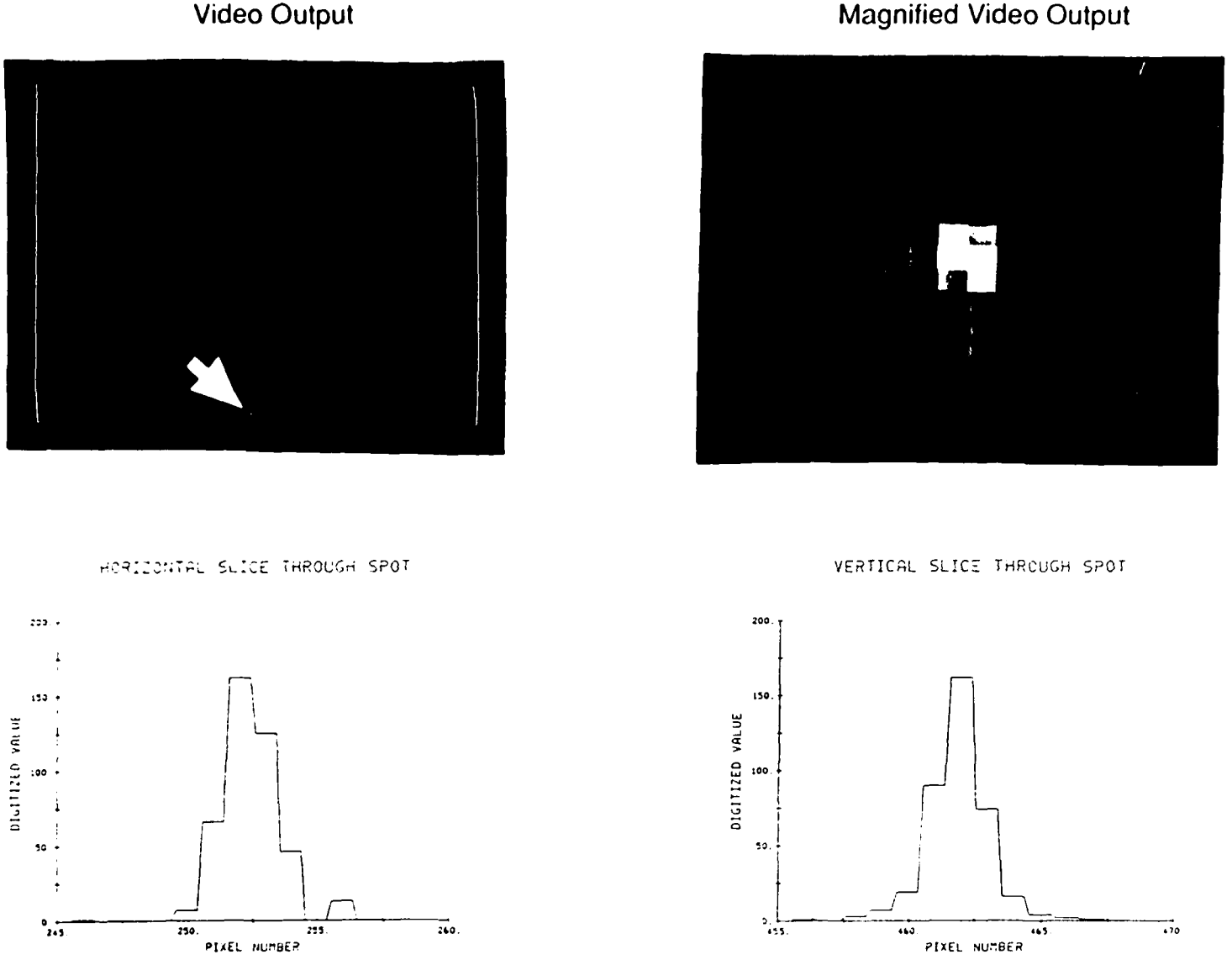

(d) Output of laser receiver for incident angles $\theta_x = 0°$ $\theta_y = -15°$

Figure 18. (Continued) Focussing performance of holographic wide angle lens.

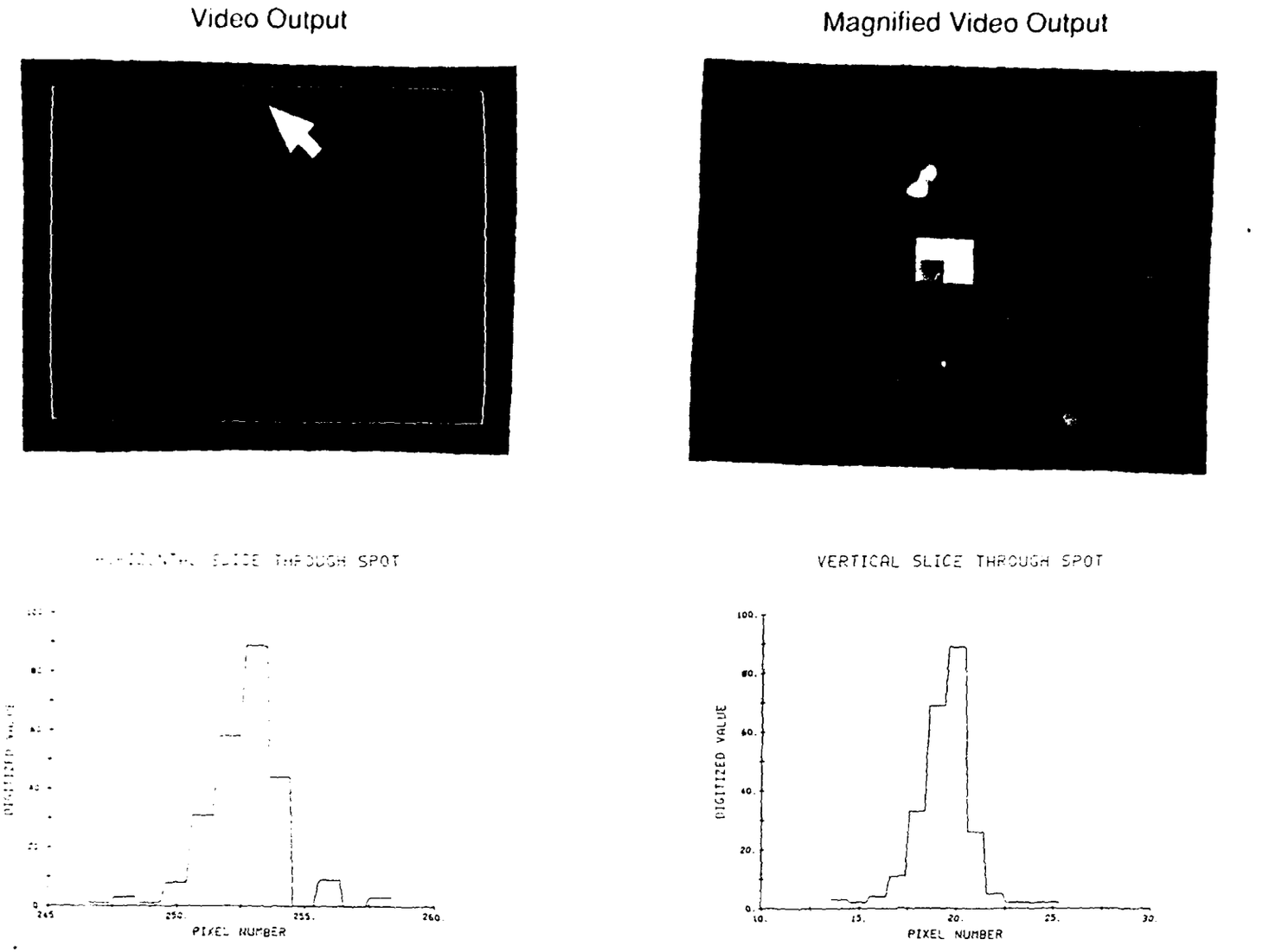

(e) Output of laser receiver for incident angles $\theta_x = 0°$ $\theta_y = 15°$

Figure 18. (Continued) Focussing performance of holographic wide angle lens.

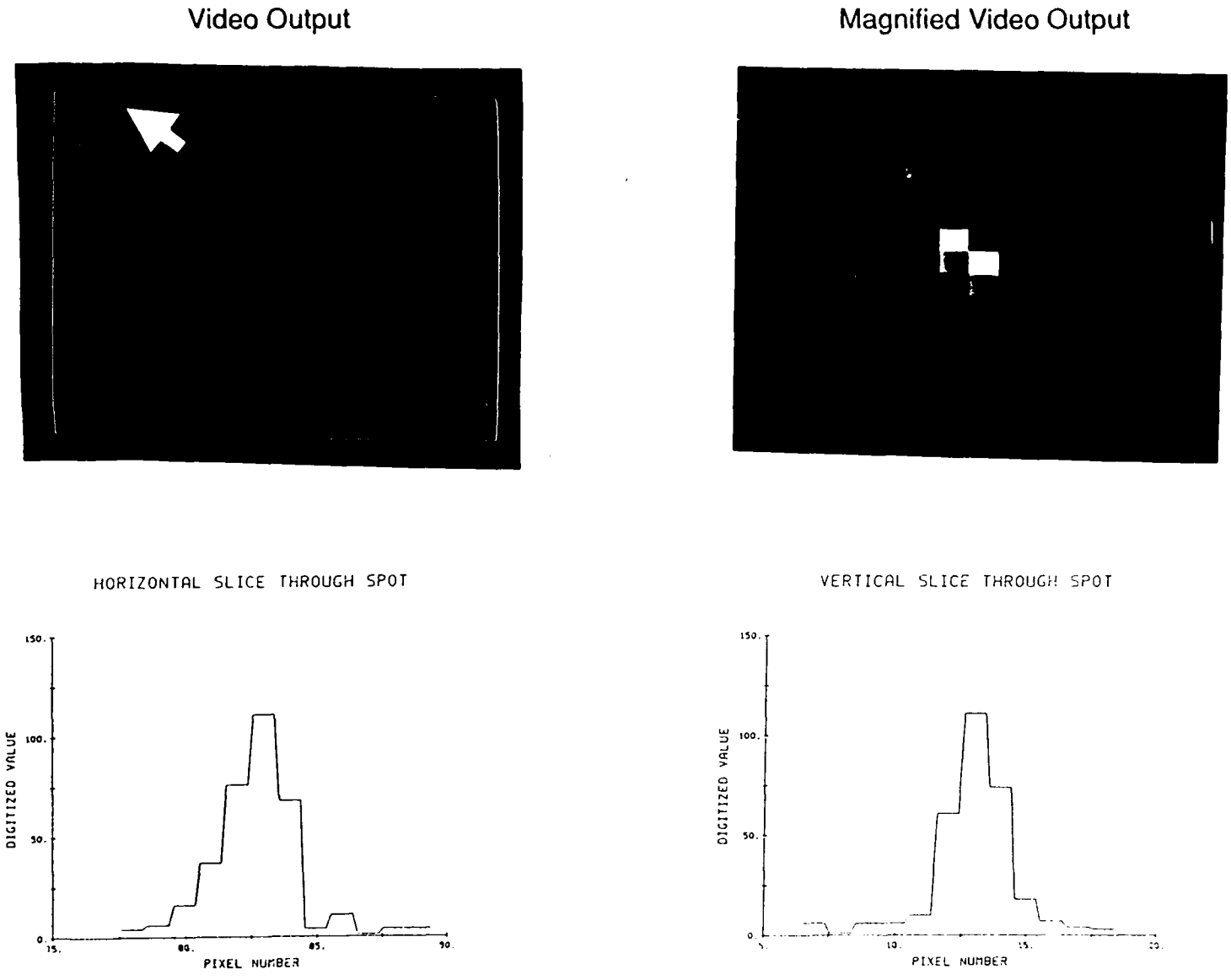

(f) Output of laser receiver for incident angles $\theta_x = -15°$ $\theta_y = 15°$

90-10018

Figure 18. (Continued) Focussing performance of holographic wide angle lens.

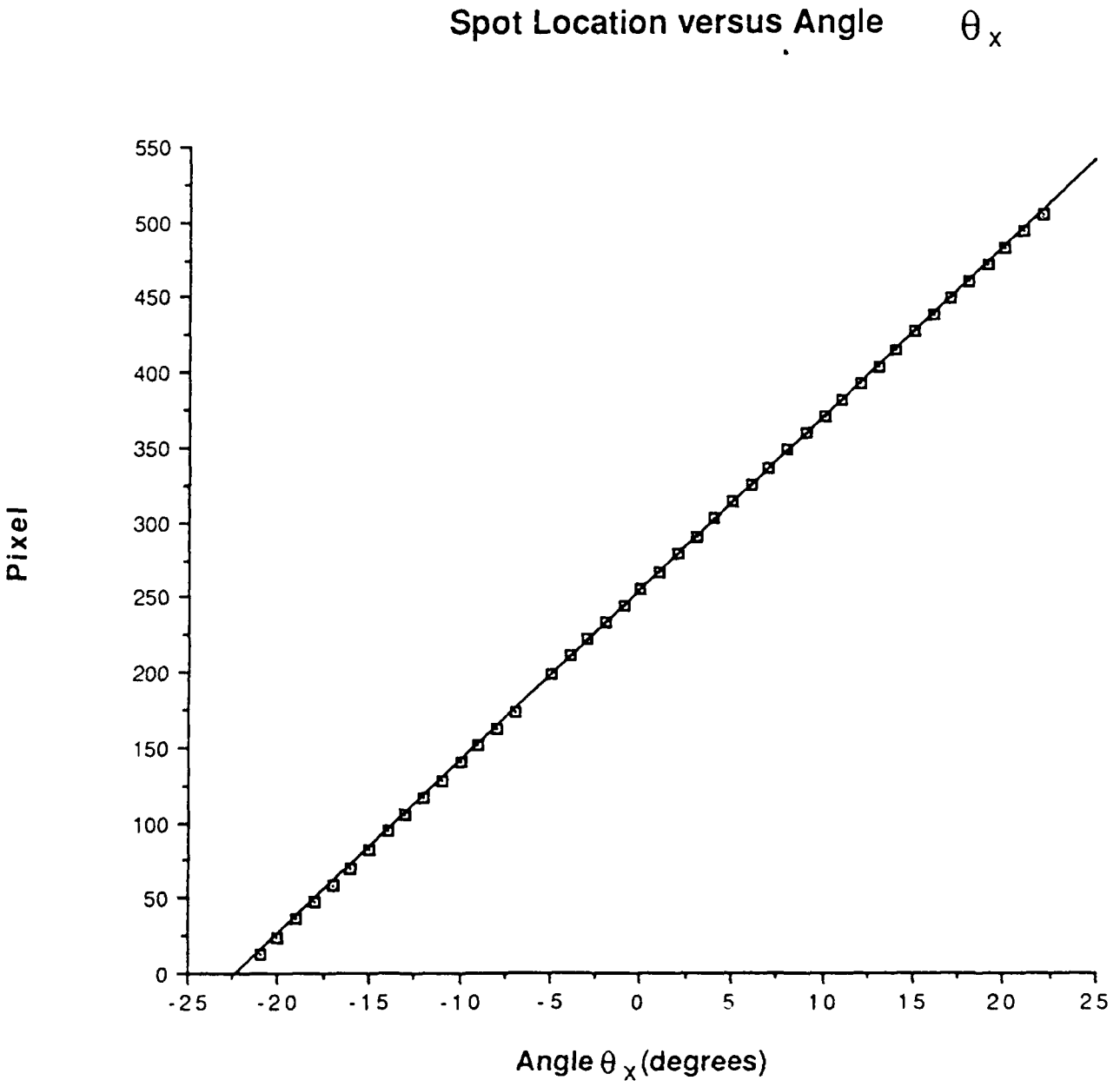

Figure 19. Spot location as a function of incident beam angle in the X-direction.

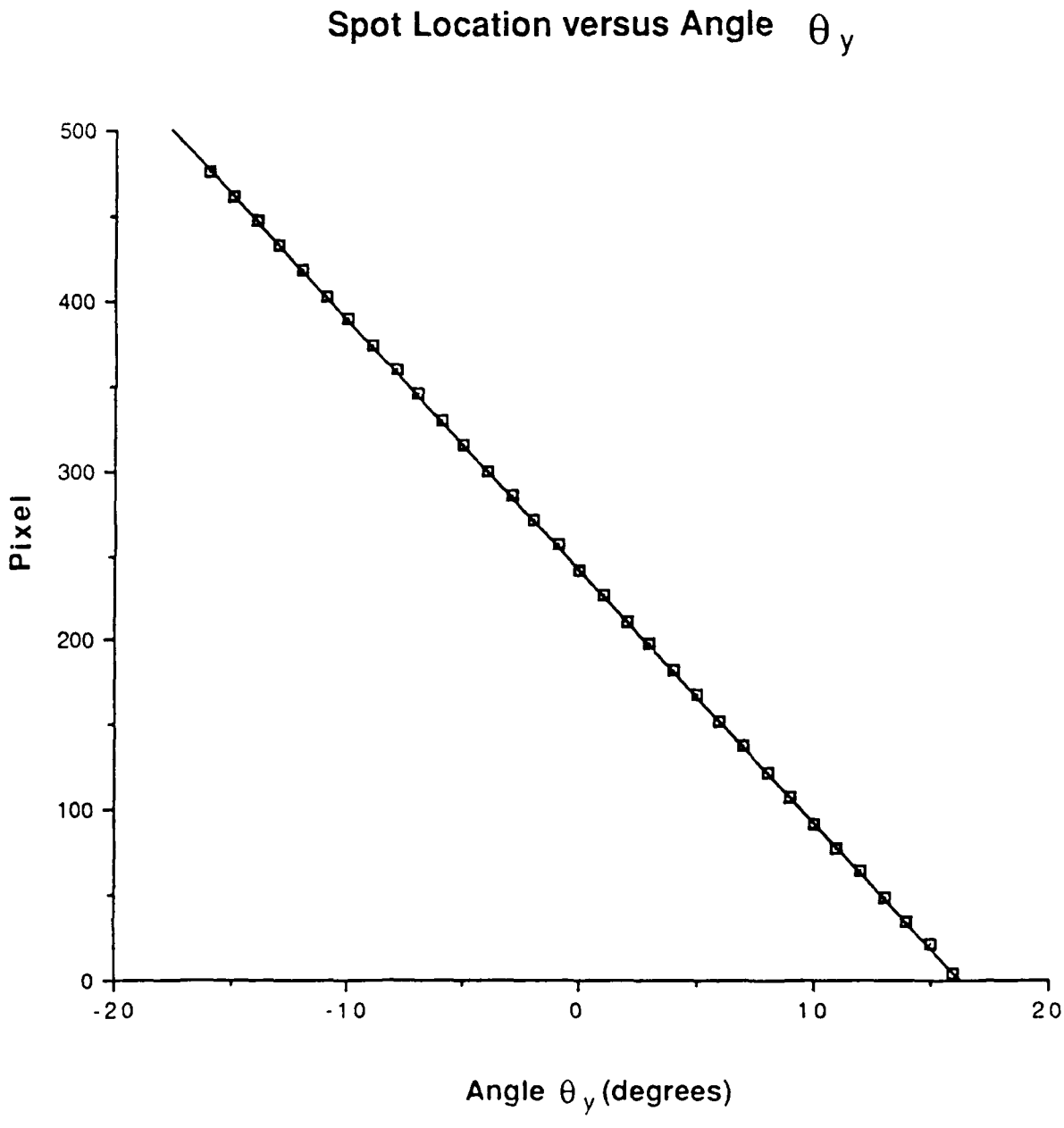

Figure 20. Spot location as a function of incident angle in the Y-direction.

locations limited the positional accuracy to ±0.5 pixel. The corresponding angular resolution is about 0.065° or 1.1 mrad which is more than adequate for this application. The accuracy can be further improved by interpolating the output to determine the centroid location of the focussed spot. With the use of interpolation, the incident angle of a laser beam can be determined with an accuracy as high as 0.2 mrad.

The efficiency of the holographic lens was measured to be only 25%, about a factor of two below what can be achieved (see Section 3). The large wavelength shift between recording and playback made it difficult to determine the proper exposure level. The holograms were slightly under-exposed which resulted in a lower efficiency (peak efficiency of the individual hologram was about 70% of the design goal).

To achieve high signal-to-noise ratio, the detector array should be driven to near saturation by the focussed beam. At 75% saturation, the input light power through the 5mm aperture was measured to be about 10nW (irradiance at aperture = $50nW/cm^2$). To put this in perpective, a 25mW laser source expanded to a beam diameter of 8m would provide enough light power for unambiguous detection.

This page intentionally left blank.

7.0 SUMMARY AND RECOMMENDATION

A wide-angle holographic lens was designed and fabricated for use in a wide FOV laser communication receiver. Besides providing wide FOV performance, advantages offered by the holographic approach include light weight, compact packaging that leaves room for E-O modulator and atomic filter, minimal effect on the aerodynamics and radar cross-section of the platform, and design flexibility. For comparison, a wide-angle conventional lens fabricated with multiple spherical glass elements is shown in Figure 21(a) and the holographic counterpart is shown in Figure 21(b). Not included in the drawings are the mounting hardware which further increases the bulkiness of the conventional lens design. Note also that with the restricting aperture inside the multi-element lens, a laser receiver utilizing a conventional lens would require a larger cut-out on the surface of the airborne platform.

The holographic lens utilized a Fourier transform geometry with the restricting aperture at plane of the input window which minimized the size of the cut-out that has to be made on the platform. The effective f/number of the holographic lens was f/2.4. It was designed to provide a uniform spot focussed spot over a 52° FOV with a constant rms spot diameter of $20\mu m$. The spot diameter corresponded to a width of 1.5 detector pixels which permitted interpolation to achieve an angular resolution better than 1.1 mrad. The holographic lens fabricated in the program satisfied all design goals except for efficiency which was a factor of 2 lower than expected. The lower efficiency was due to the underexposure of the holograms. The large shift between recording and playback wavelengths made it more difficult to estimate the correct exposure level. It was not a fundamental problem and can certainly be solved given enough time and funding to optimize the recording process.

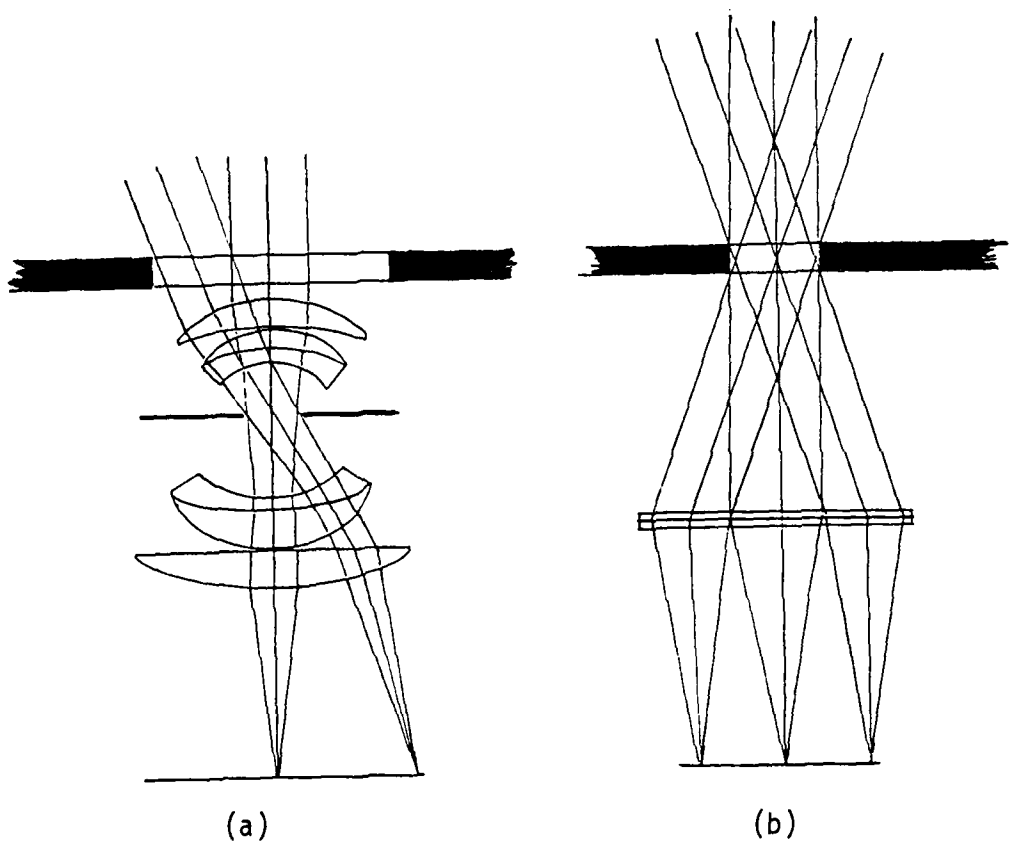

Figure 21. Conventional and holographic implementations of wide FOV lens.
(a) Conventional lens with multiple spherical glass elements.
(b) Holographic lens.

The design approach can be extended to a wider FOV. Using the same basic design approach but with the phase function optimized for higher off-axis angles, preliminary analysis indicated that a holographic lens with a 90° FOV can be fabricated by allowing the spot diameter to increase to about 30μm. It should be noted that with the use of interpolation to determine the spot location, the larger spot diameter may not have a significant effect on the angular resolution of the laser receiver as long as the focussed spot remains circularly symmetric and enough optical power is available to drive the detector array to near saturation.

With the basic concept demonstrated, the following tasks are recommended for near term development to bring the holographic laser transmitter/receiver closer to an operational system.

1) Develop a complete strategy for acquisition and tracking. Issues such as optimum scan pattern and scan rate in the acquisition mode, number and placement of transmitters/receivers around the platform, and the hand off procedure between the acquistion and tracking modes should be addressed. The strategy can initially be validated via simulation.

2) Design and fabricate a holographic laser receiver with a 90° FOV.

3) Design and fabricate a holographic laser transmitter with a 90° FOV.

4) Demonstrate acquisition and tracking between two communication transmitters and receivers on separate moving platforms.

This page intentionally left blank.

8.0 REFERENCES

1. Jordan Jr., J.A., P.M. Hirsch, L.B. Lesem and D.L. Von Rooy, "Kinoform Lenses," Appl. Opt. 9, p. 1983, 1970.

2. Swanson, G.J., and W.B. Veldkamp, "Infrared Applications of Diffractive Optical Elements," in Proceedings of SPIE, Vol. 884, Computer Generated Holography II, ed. S.H. Lee, p. 100, 1988.

3. Buralli, D.A., G.M. Morris and J.R. Rogers, "Optical Performance of Holographic Kinoforms," Appl. Opt. 28, p. 976, 1989.

4. Fairchild, R.C., and J.R. Fienup, Computer-originated Aspheric Holographic Optical Elements," Opt. Eng. 21, p. 133, 1982.

5. Moharam, M.G., and T.K. Gaylord, "Rigorous Multi-wave Analysis of Planar Grating Diffraction," J. Opt. Soc. Am., 71, p. 811, 1981.

6. Kogelnik, H., "Coupled Wave Theory for Thick Hologram Gratings," Bell Syst. Tech. J., 48, p. 2909, 1969.

7. Welford, W.T., Aberrations of Symmetrical Optical System, Chapter 7, Academic Press, New York, 1974.

8. Assenheimer, M., et al., "Recursive Design for an Efficient HOE with Different Recording and Readout Wavelengths," Appl. Opt., 27, p. 4747, 1988.